Project No. 15-2762
August 1, 1992

A final report for

MODELING THE JOVIAN AURORA

Submitted to:

Dr. J. Bergstrahl
Planetary Atmospheres Section
Code SL
NASA Headquarters
Washington, DC 20546

Submitted by:

J. Hunter Waite, Jr.
Southwest Research Institute

SOUTHWEST RESEARCH INSTITUTE
Instrumentation and Space Research Division
6220 Culebra Road, San Antonio, Texas 78238
(512) 684-5111 • FAX (512) 647-4325

Project No. 15-2762
August 1, 1992

A final report for

MODELING THE JOVIAN AURORA

Submitted to:

Dr. J. Bergstrahl
Planetary Atmospheres Section
Code SL
NASA Headquarters
Washington, DC 20546

Submitted by:

J. Hunter Waite, Jr.
Southwest Research Institute

APPROVED:

J. L. Burch

James L. Burch, Vice President
Instrumentation and Space Research Division

SOUTHWEST RESEARCH INSTITUTE
Instrumentation and Space Research Division
6220 Culebra Road, San Antonio, Texas 78238
(512) 684-5111 • FAX (512) 647-4325

TABLE OF CONTENTS

1.0 Background

The Jovian aurora is the most powerful aurora in the solar system, over 100 times more powerful than the Earth's aurora. These magnificent *visual* displays can provide important information about the planetary magnetosphere which is responsible for the acceleration of energetic particles that produce aurora at any planet. Similarities and differences in planetary auroral emissions are thus a viable means of classifying and studying both comparative atmospheric and magnetospheric processes. For instance, at Earth the solar wind is the primary source of auroral power while at Jupiter it is conjectured that the rotation of the planet is the major source of magnetospheric and auroral power. One indicator of this difference may be the type of precipitating particle responsible for the aurora. At Earth electrons play the major role while at Jupiter many researchers suspect that heavy ions (sulfur and oxygen) are the dominant auroral particles. Observations can be used to determine the identity of the particles, but in a subtle and complex way. Observations in one wavelength band such as the ultraviolet are to first order the same whether the exciting particles are electrons or ions. Yet Jupiter's aurora emits across a huge dynamic range from X ray to radio wavelengths and by combining this information important new insight into the identity of the particles and the energization processes responsible for their acceleration may be possible. However, to extract this information it is necessary to construct a model that with specified inputs from either ion or electron precipitation which is capable of calculating the observed output at X ray, ultraviolet, and infrared wavelengths. The purpose of this IR project was to develop such a model: 1) for use in interpreting the existing set of multispectral observations of Jupiter's aurora and 2) to design new experiments based on the findings to improve understanding of the underlying auroral processes.

2.0 Approach

The project plan was to use existing models of ultraviolet auroral emission signatures from both electrons and ions that had been previously developed by the Principal Investigator and his coworkers (produced in previous years under this NRA project) and add to them the capability for calculating the associated X ray and infrared emission processes. Significant upgrade to the aeronomical data associated with ultraviolet emission processes and the energy range coverage of the superthermal electron transport computer code were also completed as part of the proposed work plan. In addition, a new computer model to calculate the Doppler-shifted Lyman alpha production due to precipitating protons was used for quantifying the auroral proton precipitation. Heavy ions were modeled as well, using codes developed in past year under this program. Appropriate inputs for particle energies and fluxes were determined using the results of over 10 years of Jupiter auroral observations with the NASA/ESA International Ultraviolet Explorer satellite. These inputs included the observed changes in auroral activity that occur as a function of the rotational phase of the planet. The model was run in a time dependent manner to characterize the emission changes as a function of incoming particle identity, energy, and flux and associated rotational phase. Calculations were performed on a CRAY YMP through a grant from the University of Illinois NSF/NCSA supercomputer facility. Finally, the model results were compared to new observations in the ultraviolet (Hubble Space Telescope) and X ray (Roentgensatellite) obtained by the PI as a co-Investigator on Guest Observing programs.

3.0 Accomplishments

The specified modifications to the model provide for time-dependent (rotational phase) calculations of multiwavelength auroral emission which can be compared to existing and future observational data sets. The calculated emissions include X rays (K-shell for heavy ions and Bremsstrahlung for electrons); Lyman alpha (high resolution line shapes), H_2 Lyman and Werner band ultraviolet emissions; H_3^+ vibrational and rotational emissions, and hydrocarbon (CH_4, C_2H_2, and C_2H_6) vibration rotation emissions in the infrared. These calculations can be carried out for precipitating particles (electrons or heavy ions) with arbitrary energy distributions and influx intensity. Results to date have been compared to: 1) the ROSAT X ray observations of Jupiter to determine the role of Bremsstrahlung electrons, 2) the ultraviolet measurements of IUE and HST to examine the spectral and intensity changes as a function of planetary rotational phase 3) the comparison of Lyman alpha model profiles with IUE observations to determine the relative role of protons in the aurora, and 4) the NASA Infrared Telescope Facility measurements of H_3^+ and hydrocarbons. Particularly noteworthy are the comparisons with NASA Hubble Space Telescope measurements and NASA/ESA Ulysses Jupiter flyby data. Adaptations of the model to the Saturn system will also be undertaken to support the wide range of NASA Cassini activities presently being carried out at SwRI.

The purpose of the final report is to report the technical findings of the project. Four talks were given on the initial modeling project: 1) a talk on electron Bremsstrahlung X ray production at the annual American Astronomical Society, Division of Planetary Studies meeting in October of 1990 in Charlottesville, Virginia, 2) a poster on proton precipitation at the May, 1991 American Geophysical Union meeting in Baltimore, Maryland, 3) an invited paper on multi-spectral time dependent modeling at the International Union of Geodosy and Geomagnetism in Vienna in August of 1991, and 4) a paper entitled "Jovian Bremsstrahlung X Rays: A Ulysses Prediction" at the annual meeting of the Division of Planetary Studies of the American Astronomical Society held in Palo Alto in November of 1991. The fourth paper predicted the Jovian auroral X ray flux that should be measured by the Ulysses Gamma Ray Burst experiment during the Ulysses spacecraft's closest encounter with Jupiter in February of 1992. This paper generated much interest from people studying the Jovian aurora and from experimenters on the Ulysses spacecraft. As a result of this interest two things happened: 1) a paper of the same title was submitted and accepted for publication in the January issue of the Geophysical Research Letters, and 2) a massive observing campaign was organized to provide supporting ultraviolet and infrared observations at the time of the Ulysses encounter. This observational interest allowed personnel at SwRI (Alan Stern, PI; Hunter Waite Co-I) to obtain director's discretionary time on the Hubble Space Telescope to support the Ulysses encounter by obtaining ultraviolet observations. The multiple wavelength observations obtained during the Ulysses encounter in February were analyzed using the auroral model developed under this project and the exciting new results were reported in two invited papers that were presented this summer: 1) the Magnetospheres of the Outer Planets Goertz-Smith Memorial symposium held at UCLA June 22-26, 1992 and 2) the International Workshop on Variable Phenomena in Jovian Planetary Systems held in Annapolis, MD July 13-16, 1992.

4.0 Technical Reports

4.1 Model Modifications

Substantial progress was made to the Jovian Aurora Model during the course of this project. A general description of the model can be found in Waite et al. [1983]. Specific improvements incorporated into the model include the following:

- New cross sections for electron impact on H_2 are used for calculating the resulting dissociation and excitation states of H_2 and its products.
- Refined energy budget for the production and loss of heat in the atmosphere, including dissociative, rotational, and vibrational excitation of H_2, consistent with the new electron impact cross section data.
- Preliminary calculation of infrared emissions from the molecule, H_3^+, for comparing to recent observations of Jupiter's auroral region at these wavelengths.
- An improved temperature-pressure relationship has been constructed subject to recent observational constraints at three altitudes in the Jovian atmosphere.
- The production of bremsstrahlung X rays from precipitating auroral electrons within Jupiter's atmosphere for comparison to recent observations.

In this report, these five areas of improvements will be discussed in detail as they have not already been covered in the attached papers.

4.1.1 New Electron Impact Cross Sections for H_2

The auroral electron distributions as a function of altitude and energy are found by using a two-stream electron transport code for Jupiter as described in Waite et al. [1983]. At non-relativistic energies (below 10 keV), the electron-induced H_2 ultraviolet band emissions are calculated using the most recent cross sections of Ajello et al. [1984] and Shemansky et al. [1985]. Emissions from the singlet (B, B', and C) and triplets (B", D, and D') states are calculated, as well as the cascade contributions to the Lyman band from the E, F states. The Lyman band system arises from (B-X) transitions while the Werner band system is produced by (C-X) transitions. Additionally, dissociative excitations (both direct and predissociation) of H_2 are important in the accounting of the total cross section and the overall energy budget. These dissociations have been included in the present model and give rise to Lyman α and Lyman β emissions. It is well known that there are two distinct groups of energy distributions of H atoms formed on dissociative excitation of H_2. These groups are referred to as "fast" and "slow", with energy peaks at about 4 and 0.3 eV, respectively. To calculate these groups, we have used the recent cross sections of Ajello et al. [1991] with the most recent corrections for absolute laboratory reference calibration at 100 eV from Gladstone [private communication, 1991]. We have begun a collaboration with Dr. R. Gladstone (UCB) who used our model results as input to his radiative transfer model to compute the Lyman α intensity distribution in the Jovian aurora region.

At electron energies greater than 10 keV and up to 2 MeV, the relativistic H_2 cross sections of Garvey et al. [1977] have been employed (using clarifications by Porter et al. 1976). Also included within this work are cross sections for 16 forbidden states and the ionization cross section that we calculate in addition to the allowed Rydberg states described above. The relativistic cross sections have been normalized to the non-relativistic values at 10 keV to ensure consistency. These basic data have been added to the XSECT program which generates the cross section information used as input to the Jovian aurorae code.

Optical depth effects have been included in the model which attenuate the newly produced ultraviolet emissions. We have attempted to account for the effects of slant path through the atmosphere on the emerging ultraviolet radiation that is observed. These new developments are further explained in the attached paper by Waite et al. [1992].

4.1.2 Improved Energy Budget

The treatment of the neutral heating of the atmosphere in the model has been expanded to include source terms for the direct dissociative excitation and predissociation of H_2 from Rydberg and forbidden levels. The cross sections for these processes are consistent with the new data described above for the production of the "fast" and "slow" H atom components.

4.1.3 Infrared Emissions from H_3^+

Infrared observations of the auroral zone of Jupiter are playing an increasingly important role in understanding the nature and morphology of auroral processes. Recent observations of the global distribution of H_3^+ emissions at 2 and 4 μm by Baron et al. [1991], Kim et al. [1991] and Drossart et al. [1992] contain key information on the current dissipation and particle precipitation in the upper atmosphere. To this end, we have made a preliminary effort to include key infrared emissions from H_3^+ within the Jovian auroral model.

Additional H_3^+ chemistry was added to the code to include three distinct forms of the H_3^+ ion: the newly created ion in a high energy, linear form; the excited form of the more stable cyclic ion; and the ground state cyclic ion. Following work of Kim [1988], two modes of vibration are considered with details of the 6 lowest states included in the code. A preliminary development for the distribution of energy in the nascent H_3^+ population was implemented using the assumption of local thermodynamic equilibrium (LTE). If radiative effects turn out to be important at higher levels in the atmosphere, then this development will break down and non-LTE effects will need to be considered. This was outside the scope of this IR and has been included in a new proposal submitted to the NASA Planetary Atmospheres Program.

4.1.4 Improved T-P Profile in the Auroral Atmosphere

We have improved the neutral thermal profile in the Jovian auroral region that is used in the model by considering recent observations in the infrared, ultraviolet, and X ray. Previously, we had used a thermal profile appropriate for the Jovian equatorial region based on Voyager observations. The new profile is the first attempt at characterizing the auroral thermal structure and has drawn considerable interest in the planetary community. It is based on

hydrocarbon emissions from CH_4 and C_2H_2 observed by Voyager IRIS in the lower thermosphere (above 1 bar) in the auroral zone [Drossart et al., 1992]. This serves as the major sink of heat from auroral particle and Joule heating in the energy budget. In the middle thermosphere (1 to 0.01 μbar pressure level), the neutral temperature profile is constrained by observations of H_2 quadrupole emission [Kim et al. 1990]. This region of the atmosphere is a pivotal point for the thermal structure and helps to define the thermal gradient and conductive heat transport within the atmosphere. The third and last constraint on the thermal profile is in the upper thermosphere (pressures below about 0.01 μbar) and is due to infrared emissions from the H_3^+ ion [Drossart et al., 1992]. Its density and necessary heating are intimately linked to the region of particle precipitation and, thus, aids in characterizing the source of the auroral particle heating. We have joined these three constraints with a Bates profile [Gladstone, private communication, 1992] as an initial attempt to characterize the thermal structure of the Jovian auroral zone. In collaboration with Dr. P. Drossart (Obs. de Paris, Meudon), the Bates parameters have been adjusted for consistency the CH_4 band emission in the auroral zone. This work was partially reported at the International Workshop on Variable Phenomena in Jovian Planetary Systems held in Annapolis, MD, during 13-16 July, 1992.

4.1.5 New Bremsstrahlung X Ray Calculations

The scope of the Jovian aurora code has been expanded to include the production of bremsstrahlung X rays by precipitating auroral electrons. The differential bremsstrahlung cross sections were taken from the work of Koch and Motz [1959] who used the nonrelativistic Bethe-Heitler formulation, averaged over outgoing photon emission angles. A variety of analytic forms have been used to describe the electron energy spectrum appropriate for bremsstrahlung calculations. We use the form suggested by Barbosa [1990],

$$J(E) = J_0\left(\frac{E_0}{E}\right)^{\gamma}\exp\left(\frac{E}{E_0}\right),$$

for the differential electron flux ($cm^{-2}s^{-1}keV^{-1}$) as it combines the power law behavior with an exponential high-energy cutoff to the spectrum at the characteristic energy E_0. In other model calculations we have also employed the simple power law form (without exponential) with parameters measured from the recent Ulysses encounter with Jupiter [Cravens, private communication, 1992]. X ray atmospheric effects have been included in the model but were less than 10% at all photon energies above 100 eV for all primary electron beam energies considered in our preliminary calculations.

In a preliminary model, calculated electron beams that are consistent with 10 years of IUE ultraviolet observations [Livengood and Moos 1990] have been used to compute bremsstrahlung X ray fluxes. These calculations served as a predictive data set for the Ulysses GRP observations. A more complete description is given in the attached paper [Waite et al. 1992]. As an update to this paper, the Ulysses encounter with Jupiter in May, 1992 did not yield data with sufficient signal-to-noise ratio to compare with our model predictions.

References

Ajello, J. M. et al., Cross sections for production of H(2p, 2s, 1s) by electron collisional dissociation of H_2, *Astrophys. J, 371*, 422-431, 1991.

Ajello, J. M. et al., Studies of extreme-ultraviolet emission from Rydberg series of H_2 by electron impact, *Phys. Rev. A., 29*, 636-653, 1984.

Barbosa, D. D., Bremsstrahlung X rays from Jovian auroral electrons, *J. Geophys. Res., 95*, 14969-14976, 1990.

Baron, R. et al., Images of Jovian auroral ovals in the 3 and 4 micron bands of H_3^+, *EOS Trans., 72*, 236, 1991.

Drossart, P. et al., *Inter. Workshop on Var. Phen. in Jovian Planet. Sys.*, 1992.

Garvey, R. H. et al., Relativistic yield spectra for H_2, *J. Appl. Phys., 48*, 4353-4359, 1977.

Kim, S. J. et al., Methane emission at 3.5 and 7.8 microns from the Jovian auroral zone, *EOS Trans., 72*, 236, 1991.

Kim, S. J. et al., Temperatures of the Jovian auroral zone inferred from 2-μm H_2 quadrupole line observations, *Icarus, 84*, 54-61, 1990.

Kim, S. J., Infrared processes in the Jovian auroral zone, *Icarus, 75*, 399-408, 1988.

Koch, H. W. and J. W. Motz, Bremsstrahlung cross-section formulae and related data, *Rev. Mod. Phys., 31*, 920, 1957.

Livengood, T. A. and H. W. Moos, Jupiter's north and south polar aurora with IUE data, *Geophys. Res. Lett., 17*, 2265-2268, 1990.

Porter, H. S. et al., Efficiencies for production of atomic nitrogen and oxygen by relativistic proton impact in air, *J. Chem, Phys., 65*, 154-167, 1976.

Shemansky, D. E. et al., Electron impact excitation of H_2: Rydberg band systems and the benchmark dissociative cross section for H Lyman-alpha, *Astrophy. J., 296*, 765-773, 1985.

Waite, J. H., Jr. et al., *Inter. Workshop on Var. Phen. in Jovian Planet. Sys.*, 1992.

Waite, J. H., Jr. et al., Electron precipitation and related aeronomy of the Jovian thermosphere and ionosphere, *J. Geophys. Res., 88*, 6143-6163, 1983.

4.2 Model Results

Two papers have been published in refereed journals reporting the work and three more are presently in preparation. The abstract for each paper is presented below and the complete publication can be found in the appropriate section of the appendix.

4.2.1 Comment on "Bremsstrahlung X Rays from Jovian Auroral Electrons"

The subject of this comment is a recent paper by D. D. Barbosa in which it is argued that Electron bremsstrahlung is the most likely source of the auroral X ray emissions that have been observed at Jupiter [Barbosa, 1990]. Barbosa bases his argument on observational and theoretical studies of the production of secondary electrons in the Earth's aurora. As this comment will show, however, Barbosa's interpretation is flawed because it ignores the constraint that the primary electron distribution parameters place on the parameters for the secondary electron distribution. As a result, Barbosa's postulated secondary electron fluxes are over 3 orders of magnitude greater than the theory of auroral electrons permits. (see Appendix A)

4.2.2 "Jovian Bremsstrahlung X Rays: A Ulysses Prediction"

The Jovian aurora is the most powerful planetary aurora in the solar system; to date, however, it has not been possible to establish conclusively which mechanisms are involved int he excitation of the auroral emissions that have been observed at ultraviolet, infrared, and soft X ray wavelengths. Precipitation of Iogenic heavy sulfur and oxygen ions, downward acceleration of electrons along Birkeland currents, and a combination of both of these mechanisms have all been proposed to account for the observed auroral emissions. Modeling results reported here show that precipitating auroral electrons with sufficient energy to be consistent with the Voyager UVS observations will produce bremsstrahlung X rays with sufficient energy and intensity to be detected by the Solar Flare X Ray and Cosmic Ray Burst Instrument (GRB) on board the Ulysses spacecraft. The detection of such bremsstrahlung X rays at Jupiter would provide strong evidence for the electron precipitation mechanism, although it would not rule out the possibility of some heavy ion involvement , and would thus make a significant contribution toward solving the mystery of the Jovian aurora. (see Appendix B)

4.2.3 "The Role of Proton Precipitation in Jovian Aurora: Theory and Observation"

This paper presents the development of a Jovian proton aurora model. It utilizes the continuous loss method, and local charge state equilibrium of the ion/neutral beam at each altitude in conjunction with the more recent cross sections for Lyman alpha production by energetic hydrogen and protons to calculate the expected Lyman alpha spectral line profile. Particle energy spectra consistent with those measured by the Voyager Low Energy Particle Telescope (LEPT) in the Jovian magnetosphere were then used as inputs and the model results compared to International Ultraviolet Explorer Lyman alpha line profile data at high Jovian latitudes. The comparison allows an upper limit of 10% to be set for the role of proton precipitation in producing the observed ultraviolet aurora. (see Appendix C)

4.2.4 "Lyman Alpha Line Shapes from Electron Impact H_2 Dissociative Processes in the Jovian Auroral Zone"

The results reported in this paper define the Lyman alpha line profile generated as a result of electron impact on H_2. The primary point of interest is the role of fast and slow H atoms from dissociative excitation processes in defining the shape of the line profile. Some comparison to existing IUE Lyman alpha line profiles is also discussed. (see Appendix D)

4.2.5 "Multispectral Observations of the Jovian Aurora: ROSAT and HST"

Recent results from Hubble Space Telescope (HST) ultraviolet images and Roentgensatellite (ROSAT) X ray spectral data are reported in this paper. Comparison to previous observations, modeling of auroral processes, and recent Ulysses/Jupiter in situ data suggest a new paradigm for Jupiter auroral processes, which is much more Earth-like than previously thought from Voyager data. (see Appendix E)

APPENDIX A

JOURNAL OF GEOPHYSICAL RESEARCH, VOL. 96, NO. A11, PAGES 19,529–19,532, NOVEMBER 1, 1991

Comment on "Bremsstrahlung X Rays From Jovian Auroral Electrons" by D. D. Barbosa

J. H. WAITE, JR

Space Sciences Department, Southwest Research Institute, San Antonio, Texas

The subject of this comment is a recent paper by D. D. Barbosa in which it is argued that electron bremsstrahlung is the most likely source of the auroral X ray emissions that have been observed at Jupiter [*Barbosa*, 1990]. Barbosa bases his argument on observational and theoretical studies of the production of secondary electrons in the Earth's aurora. As this comment will show, however, Barbosa's interpretation is flawed because it ignores the constraint that the primary electron distribution parameters place on the parameters for the secondary electron distribution. As a result, Barbosa's postulated secondary electron fluxes are over 3 orders of magnitude greater than the theory of auroral electrons permits.

BACKGROUND

The identity of the particles involved in Jovian auroral activity has not been conclusively established and remains a subject of some controversy. Data relevant to this question comprise both observations of auroral emissions obtained by remote sensing at X ray, UV, IR, and radio wavelengths and in situ particle measurements made by the energetic particle detectors on Voyager. These data do not permit the identification of any one single source for the Jovian auroral emissions. The UV data tend to point to precipitating electrons (in the energy range of 10-50 keV) as the dominant source, while the in situ measurements reported by *Gehrels and Stone* [1983] suggest that the precipitation of energetic heavy ions (oxygen and sulfur ions in the energy range of 40-1000 keV) plays an important role in auroral processes. X ray observations have also been interpreted as evidence for heavy ion precipitation [*Metzger et al.*, 1983]. *Waite et al.* [1988] have attempted to reconcile these interpretations by proposing that both electrons and ions, depositing their energy at different altitudes and latitudes, play a role in the production of the Jovian aurora. A definitive answer to the question of the particles and processes involved in the production of the aurora at Jupiter, however, will require further remote-sensing observations in the different wavelength regimes as well as the measurements to be made by Galileo when it arrives at Jupiter in early 1992.

INTERPRETATION OF THE X RAY OBSERVATIONS

As noted above, further evidence in support of the heavy ion precipitation process was provided by X ray observations of the Jovian aurora carried out by *Metzger et al.* [1983]. The energy resolution of the Einstein X ray observatory used in the observations was not sufficient to distinguish between a bremsstrahlung power law distribution and *K* shell emission line spectra from sulfur and/or oxygen. However, based on modeling the *K* shell and bremsstrahlung mechanisms and their convoluted response within the Einstein telescope, *Metzger et al.* [1983] inferred that the energy required to produce the observed X ray emission by means of electron bremsstrahlung was unreasonably large compared with that required by the *K* shell mechanism and thus argued in favor of heavy ion precipitation as the source of Jovian auroral X rays.

The conclusions of Metzger et al. have been called into question recently by the work of *Barbosa* [1990]. Barbosa states (p. 14,970) that his

> aim is to examine critically the conditions under which the X ray measurements of *Metzger et al.* [1983] can be plausibly accounted for in the framework of an electron-excited aurora. We find that electron bremsstrahlung gives a most credible explanation of the X ray data and one which is consistent with electron generation of UV, infrared, and radio emissions from the auroral regions as well. The main conclusion drawn from the analysis is that the precipitating auroral electrons should have a beamlike distribution in energy which evolves into an isotropic distribution with a bump on the tail in the maximum emissivity layer. This result implies the existence of field-aligned potential drops above the auroral region which give rise to characteristic electron energy spectra similar to those observed over the terrestrial aurora [*Frank and Ackerson*, 1971]. The theory here relies heavily on auroral electron measurements made at Earth [*Rees and Maeda*, 1973] and corresponding theories of such measurements [*Banks et al.*, 1974; *Evans*, 1974] for its proper interpretation in terms of primary and secondary auroral electrons.

The purpose of this comment is to present electron transport calculations similar to those performed for the terrestrial aurora by *Banks et al.* [1974]. These calculations will demonstrate the inconsistency between the primary and secondary electron distribution parameters chosen by *Barbosa* [1990]. The decreased magnitude of secondary electron fluxes that results from calculations using the transport equations suggests that electron bremsstrahlung is not likely to be the source of Jovian X rays if terrestrial auroral electron theory is applicable.

MODEL

A self-consistent calculation of the primary and secondary precipitating electron distributions forms the basis for the two-stream electron transport calculation used in the present model, which is derived from a Jovian auroral electron model introduced by *Waite et al.* [1983]. The model solves the one-dimensional chemical diffusion equations for atomic hydrogen, the major hydrocarbon species CH_4, C_2H_2, C_2H_4, C_2H_6, and CH_3, and the major ionospheric species H^+ and H_3^+. The neutral temperature

Paper number 91JA02143.
0148-0227/91/91JA-02143$02.00

structure adopted in the present study is an equatorial profile determined from the Voyager ultraviolet spectrometer occultation experiments [*Festou et al.*, 1981]. Although auroral energy input is expected to modify this profile, there is at present little indication as to the effects of this input. Furthermore, increases in the auroral thermal structure produce little change in the calculations apart from changes in the relative altitude scale of the atmosphere. Hydrocarbon results are consistent with the recent work of G. R. Gladstone and M. Allen (private communication, 1990) using an eddy diffusion coefficient at the homopause (K_h) of 2×10^6 cm^2 s^{-1}. However, the presence of hydrocarbons has no effect on the present work apart from acting as an appropriate guide in determining the valid range of the primary electron beam parameters based on the relative absorption of H_2 band emissions by hydrocarbon species [*Livengood et al.*, 1990].

The auroral electron distributions as a function of altitude and energy are found by using a two-stream electron transport code modified for Jupiter [*Waite et al.*, 1983] and extended to electron energies of 2 MeV using the relativistic H_2 cross sections of *Garvey et al.* [1977]. Input parameters of the primary incident electron distribution were chosen to be consistent with the cases A, B, and C that were presented by *Barbosa* [1990] and are shown in Table 1. The differential bremsstrahlung cross sections were taken from the work of *Koch and Motz* [1959] (formulas 3BN and II-6). X ray absorption effects were calculated, but

TABLE 1. Auroral Electron Beam Models

Case	Parameters
A	E_{op} = (10 keV)
	E_{os} = (10 keV)
	$J_{op} = 10^8$ cm^{-2} s^{-1} keV^{-1}
	$J_{os} = 1.9 \times 10^8$ cm^{-2} s^{-1} kev^{-1}
B	E_{op} = (30 keV)
	E_{os} = (10 keV)
	$J_{op} = 10^7$ cm^{-2} s^{-1} keV^{-1}
	$J_{os} = 2.4 \times 10^7$ cm^{-2} s^{-1} keV^{-1}
C	E_{op} = (100 keV)
	E_{os} = (10 keV)
	$J_{op} = 10^6$ cm^{-2} s^{-1} keV^{-1}
	$J_{os} = 2.8 \times 10^6$ cm^{-2} s^{-1} keV^{-1}

Data are from *Barbosa* [1990]. $J(E) = J_{os}(E_{os}/E)^{\gamma} e^{-E/E_{os}} + J_{op}(E/E_{op}) e^{-E/E_{op}}$; $\gamma = 2$.

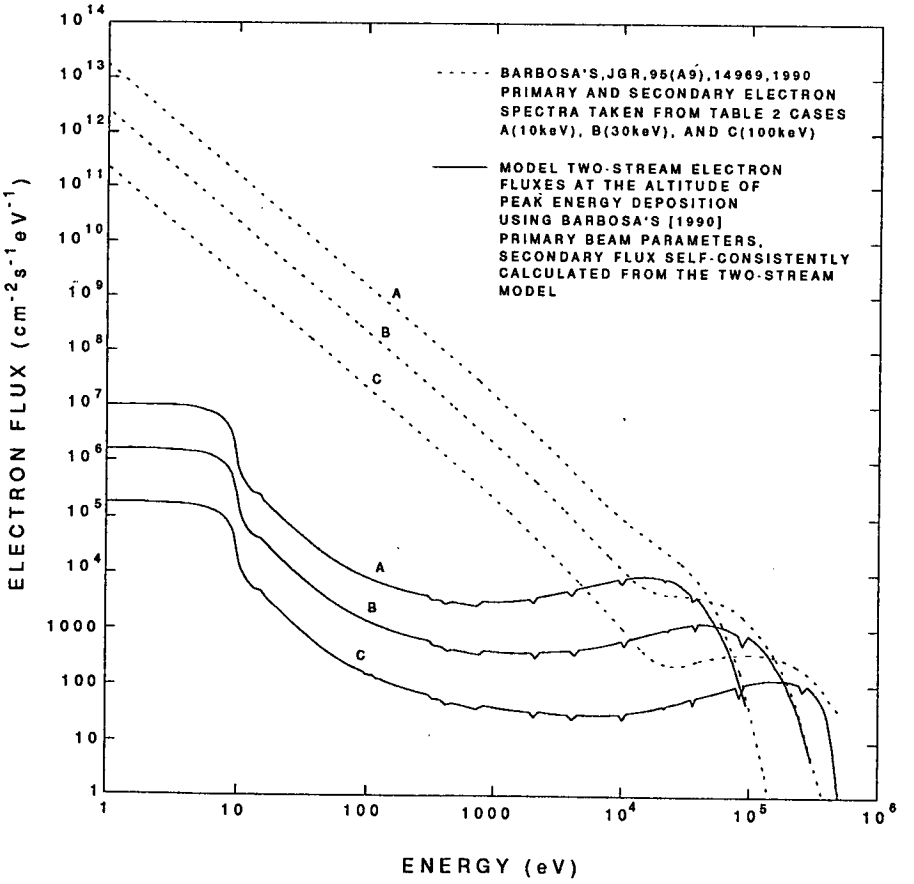

Fig. 1. Plot of the differential electron flux as a function of electron energy. The dashed lines refer to cases A, B, and C from *Barbosa* [1990]. The solid lines are from calculations using the two-stream electron transport model of Waite (this paper) with initial electron fluxes at the top of the atmosphere set by the primary beam parameters of *Barbosa's* [1990] cases A, B, and C. The small dropouts in the modeled electron fluxes are due to discrete changes in the energy bin structure and do not otherwise affect the results.

were less than 10% at all photon energies above 100 eV for the primary electron beam cases considered (10 to 100 keV).

RESULTS AND DISCUSSION

The difference between the auroral electron distribution at the altitude of peak auroral energy dissipation and that assumed by *Barbosa* [1990] is shown in Figure 1. The Barbosa distribution is over 3 orders of magnitude different from that of the two-stream electron transport calculation at an electron energy of 1 keV. The theories of auroral electron measurements [e.g., *Banks et al.*, 1974] establish a strong correspondence between the primary electron beam parameters and the secondary beam parameters, since the secondary electron spectrum is created from ionization by the primary electron beam and the collective transport of the secondary electrons formed from this process. This suggests that there exists a strong coupling between the primary electron beam parameters and the secondary electron distribution parameters within the context of terrestrial auroral theory. However, this constraint is ignored in the calculations that are presented by *Barbosa* [1990]. Table 1 is a representation of the auroral electron distribution form and the free parameters for specifying the primary and secondary electron distribution function of *Barbosa* [1990]. The primary electron beam parameters in Barbosa's study were chosen to represent both the total power constraints and the spectral characteristics of the observed H_2 band emissions [cf. *Livengood et al.*, 1990]. The secondary electron distribution parameters were then independently chosen to satisfy the observed X ray spectrum [*Metzger et al.*, 1983] while at the same time being loosely constrained by the overall power dissipation of the observed Jovian auroral emissions. However, this independent specification of the primary and secondary electron distributions is inconsistent with theoretical [*Banks et al.*, 1974] and observational [*Fung and Hoffman*, 1988] characteristics of the terrestrial aurora and corresponding electron transport calculations of the Jovian aurora presented in Figure 1.

X ray flux as a function of photon energy as seen from Earth is shown in Figure 2. The solid lines indicate the two-stream calculation, and the dotted lines the calculations of *Barbosa* [1990]. The observational data points of the Einstein Jovian X ray observations are shown by the solid circles with corresponding error bars. The excellent agreement of *Barbosa* [1990] is due to the arbitrary choice of the free parameters specifying the secondary electron distribution, the source of contention in the present comment. Note that the X ray spectrum produced by the two-stream model is both harder in spectral content and over an order of magnitude smaller in X ray intensity in the region of the Einstein X ray observations.

Similar calculations of the predicted Jovian X ray production

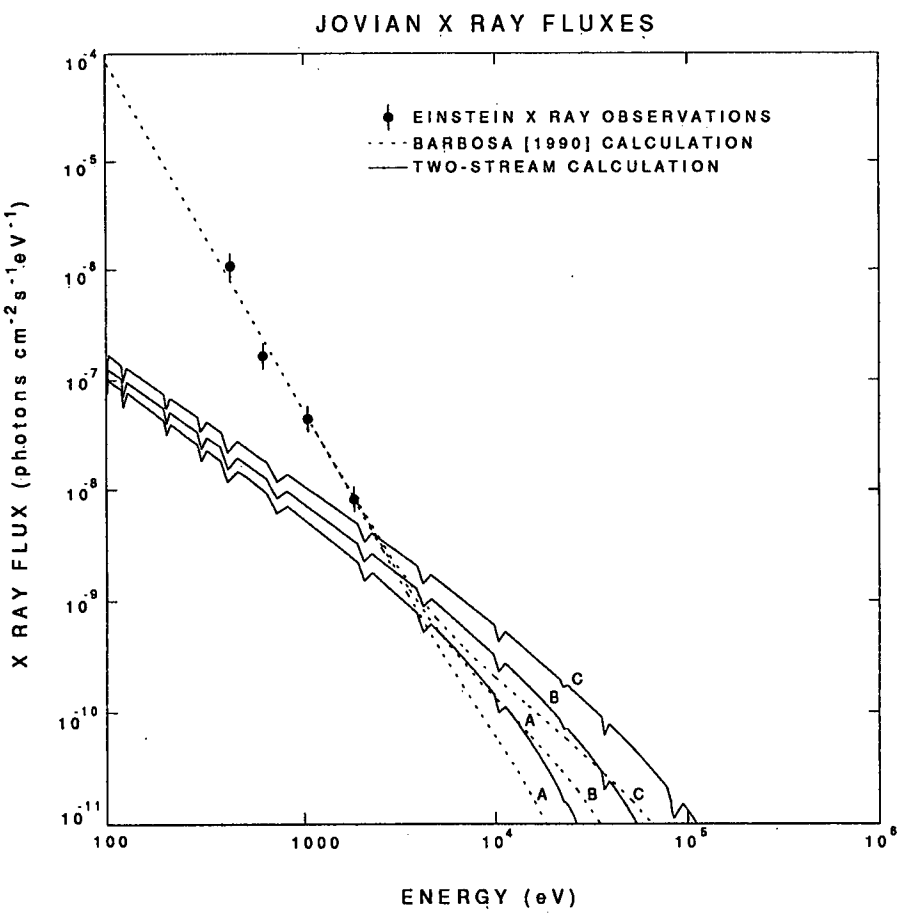

Fig. 2. Plot of the Jovian differential X ray flux as a function of photon energy as viewed from an Earth-orbiting observation platform such as Einstein. The *Metzger et al.* [1983] Einstein observations are shown by the data points, and the empirical fit of *Barbosa* [1990] by the dashed line. Results of the self-consistent model of Waite (this paper) for input cases A, B, and C are shown by the solid lines. Again the discrete changes in the energy grid introduce small dropouts that do not otherwise affect the results.

from bremsstrahlung electrons have also been carried out by M. Walt (private communication, 1991) using a more sophisticated model of the electron energy degradation and subsequent X ray production [*Walt et al.*, 1979]. The agreement between the Walt (private communication, 1991) and Waite (this model) calculations is within a factor of 2 at all energies, assuming the same energetic primary electron spectrum [*Barbosa*, 1990] and the same neutral atmosphere model described in this paper.

CONCLUSIONS

Two possibilities appear to exist that could rescue the bremsstrahlung hypothesis of Jovian X ray emissions: (1) the auroral electron energy flux during the Einstein observations exceeded 500 ergs cm^{-2} s^{-1}, a deviation of over 3 σ from the average value as determined by *Livengood et al.* [1990], and (2) the Jovian auroral secondary electron spectrum is enhanced by over 2 orders of magnitude from that expected from degradation and ionization from auroral primary electrons; whereas the terrestrial analog suggests that standard electron transport calculations explain observations of secondary electrons at Earth to better than 50% [*Fung and Hoffman*, 1988]. In addition to the changes required to increase the auroral X ray intensity to the desired levels, the calculated bremsstrahlung X ray flux also has a much harder X ray spectrum than that observed at Einstein. Preferential forward scattering of electrons at higher energies (not incorporated in the present calculations, since isotropic emissions were assumed) would have a tendency to soften the spectrum, but even so, calculations by M. Walt (private communication, 1991) indicate that significant modifications to the auroral secondary electron spectrum would be required to produce the soft spectrum observed at Einstein.

Therefore the results of the two-stream calculations reported here suggest that bremsstrahlung X rays are not the likely source of Jovian X ray emissions. However, Roentgensatellit (ROSAT) observations obtained in April 1991 [*Bagenal et al.*, 1989] should help to quantify and clarify the source of Jovian X rays. ROSAT has over a factor of 2 increase in sensitivity and in energy resolution in the energy range of interest (up to 2 keV). Clearly, additional multispectral observations (X ray, UV, IR), modeling, and in situ particle observations may be necessary to sort out the source of the Jovian auroral particles.

Acknowledgments. Partial support for this work has been provided by a NASA Planetary Atmospheres grant NAGW-1657, NASA IUE and ROSAT Observations of Jupiter's Aurora grant NAG5-1429, and by an SwRI Internal Research project 15-9634. I would also like to acknowledge helpful discussions with Martin Walt of LPARL.

REFERENCES

Bagenal, F., et al., ROSAT observations of Jovian auroral X rays, a proposal to the National Aeronautics and Space Administration for the ROSAT Guest Observer Program, Greenbelt, Md., 1989.

Banks, P. M., C. R. Chappell, and A. F. Nagy, A new model for the interaction of auroral electrons with the atmosphere: Spectral degradation, backscatter, optical emission, and ionization, *J. Geophys. Res.*, *79*, 1459, 1974.

Barbosa, D. D., Bremsstrahlung X rays from Jovian auroral electrons, *J. Geophys. Res.*, *95*, 14,969, 1990.

Evans, D. S., Precipitating electron fluxes formed by a magnetic field-aligned potential difference, *J. Geophys. Res.*, *79*, 2853, 1974.

Festou, M. C., S. K. Atreya, T. M. Donahue, B. R. Sandel, D. E. Shemansky, and A. L. Broadfoot, Composition and thermal profiles of the Jovian upper at mosphere as determined by the Voyager ultraviolet stellar occultation experiment, *J. Geophys. Res.*, *86*, 5715, 1981.

Frank, L. A., and K. L. Ackerson, Observations of charged particle precipitation into the auroral zone, *J. Geophys. Res.*, *76*, 3612, 1971.

Fung, S. F., and R. A. Hoffman, On the spectrum of secondary auroral electrons, *J. Geophys. Res.*, *93*, 2715, 1988.

Garvey, R. H., H. S. Porter, and A. E. S. Green, Relativistic yield spectra in H_2, *J. Appl. Phys.*, *48*, 4353, 1977.

Gehrels, N., and E. C. Stone, Energetic oxygen and sulfur ions in the Jovian magnetosphere and their contribution to the auroral excitation, *J. Geophys. Res.*, *88*, 5537, 1983.

Koch, H. W., and J. W. Motz, Bremsstrahlung cross-section formulas and related data, *Rev. Mod. Phys.*, *31*, 920, 1959.

Livengood, T. A., D. F. Strobel, and H. W. Moos, Long-term study of longitudinal dependence in primary particle precipitation in the north Jovian aurora, *J. Geophys. Res.*, 95, 10,375, 1990.

Metzger, A. E., D. A. Gilman, J. L. Luthey, K. C. Hurley, H. W. Schnopper, F. D. Seward, and J. D. Sullivan, The detection of X rays from Jupiter, *J. Geophys. Res.*, *88*, 7731, 1983.

Rees, M. H., and K. Maeda, Auroral electron spectra, *J. Geophys. Res.*, *78*, 8391, 1973.

Waite, J. H., Jr., T. E. Cravens, J. Kozyra, A. F. Nagy, S. K. Atreya, and R. H. Chen, Electron precipitation and related aeronomy of the Jovian thermosphere and ionosphere, *J. Geophys. Res.*, *88*, 6143, 1983.

Waite, J. H., Jr., J. T. Clarke, T. E. Cravens, and C. M. Hammond, The Jovian aurora: Electron or ion precipitation?, *J. Geophys. Res.*, *93*, 7244, 1988.

Walt, M., L. L. Newkirk, and W. E. Francis, Bremsstrahlung produced by precipitating electrons, *J. Geophys. Res.*, *84*, 967, 1979.

J. H. Waite, Jr., Space Sciences Department, Southwest Research Institute, P.O. Drawer 28510, San Antonio, TX 78228-0510.

(Received January 14, 1991;
revised July 17, 1991;
accepted July 17, 1991.)

APPENDIX B

GEOPHYSICAL RESEARCH LETTERS, VOL. 19, NO. 2, PAGES 83-86, JANUARY 24, 1992

JOVIAN BREMSSTRAHLUNG X RAYS: A ULYSSES PREDICTION

J. H. Waite, Jr.[1], D. C. Boice[1], K.C. Hurley[2],
S.A. Stern[1], and M. Sommer[3]

Abstract. The Jovian aurora is the most powerful planetary aurora in the solar system; to date, however, it has not been possible to establish conclusively which mechanisms are involved in the excitation of the auroral emissions that have been observed at ultraviolet, infrared, and soft X ray wavelengths. Precipitation of Iogenic heavy sulfur and oxygen ions, downward acceleration of electrons along Birkeland currents, and a combination of both of these mechanisms have all been proposed to account for the observed auroral emissions. Modeling results reported here show that precipitating auroral electrons with sufficient energy to be consistent with the Voyager UVS observations will produce bremsstrahlung X rays with sufficient energy and intensity to be detected by the Solar Flare X Ray and Cosmic Ray Burst Instrument (GRB) on board the Ulysses spacecraft. The detection of such bremsstrahlung X rays at Jupiter would provide strong evidence for the electron precipitation mechanism, although it would not rule out the possibility of some heavy ion involvement, and would thus make a significant contribution toward solving the mystery of the Jovian aurora.

Introduction

The identity of the precipitating particles involved in Jovian auroral activity is still an open question. In situ observations of the Jovian particle populations during the Voyager 1 and 2 encounters furnished evidence for changes in the radial phase space distribution of energetic heavy ions which are best explained by ion precipitation [Gehrels and Stone, 1983]. However, the energy range of the ion measurements did not go low enough to demonstrate that heavy ion precipitation could provide the power input required to explain the ultraviolet emission intensities. Voyager provided no in situ evidence for electron precipitation; however, indications of electron acceleration in Birkeland currents connected to the auroral zone would only be observable at high latitudes closer to the planet, a region not accessible to the Voyager spacecraft.

Remote sensing observations also present a mixed picture. Soft (0.3-3.0 keV) X ray observations of the Jovian aurora by the Einstein observatory [Metzger et al., 1983] have been used to argue for heavy ion precipitation. The energy resolution of the Einstein X ray observatory was not sufficient to distinguish between a bremsstrahlung power law distribution and K-shell emission line spectra from sulfur and/or oxygen. However, based on modeling the K-shell and bremsstrahlung mechanisms and their response within the Einstein telescope, Metzger et al. [1983] inferred that the energy required to produce the observed soft X ray emission by means of electron bremsstrahlung was unreasonably large compared with that required by the K-shell mechanism and thus argued in favor of heavy ion precipitation as the source of Jovian auroral X rays. This conclusion has been substantiated by the recent electron bremsstrahlung calculations of Waite [1991]. On the other hand, attempts at observing extreme ultraviolet emissions from sulfur and oxygen precipitation were unsuccessful [Waite et al., 1988] and suggested that, although heavy ion precipitation may indeed be the source of the soft X rays, heavy ions may not have sufficient energy flux to account for the bulk of the H_2 ultraviolet emissions observed by Voyager [Broadfoot et al., 1981] and IUE [Livengood et al., 1990].

Indeed, the H_2 Lyman and Werner band emission intensities and spectral characteristics of the ultraviolet emissions can be used to set constraints on both the energy flux and energy distribution of the precipitating particles [Livengood et al., 1990]. In this paper these constraints are used in conjunction with modeling techniques to predict the hard X ray fluxes that are expected to be detected at Jupiter by the Solar Flare X Ray and Cosmic Ray Burst Instrument (GRB) as Ulysses makes its closest approach in mid-February of 1992.

Model

The auroral electron distributions as a function of altitude and energy are found by using a two-stream electron transport code modified for Jupiter [Waite et al., 1983] and extended to electron energies of 2 MeV using the relativistic H_2 cross sections of Garvey et al. [1977]. The differential bremsstrahlung cross sections were taken from the work of Koch and Motz [1959] (formulae 3BN and II-6). X ray atmospheric absorption effects were calculated, but were less than 10% at all photon energies above 100 eV for all primary electron beam energies considered. The electron transport model also calculates the electron-induced H_2 ultraviolet band emissions using the most recent cross sections of Ajello et al. [1988] and Shemansky and Ajello [1988] with the most recent corrections for absolute laboratory reference calibration [R. Gladstone, private communication, 1991].

The model also solves the one-dimensional chemical diffusion equations for atomic hydrogen and the hydrocarbon species CH_4, C_2H_2, C_2H_4, C_2H_6, and CH_3, and the major ion species H^+ and H_3^+. The neutral temperature structure adopted in the present study is an equatorial

[1]Department of Space Sciences, Southwest Research Institute, San Antonio, TX
[2]Space Sciences Laboratory, University of California, Berkeley, CA
[3]Max-Planck-Institut für Extraterrestrische Physik, Garching, Germany

Paper number 92GL00052
0094-8534/92/92GL-00052$03.00

profile determined from the Voyager ultraviolet spectrometer (UVS) occultation experiments [Festou et al., 1981]. Although auroral energy input is expected to modify this profile, there is at present limited information as to the effects of this input. Furthermore, increases in the auroral thermal structure produce little change in the calculations apart from changes in the relative altitude of the atmosphere. The hydrocarbon density profiles used in this model are consistent with the recent work of Gladstone et al. [1991] and use an eddy diffusion coefficient of 2 x 10^6 cm^2 s^{-1} at the methane homopause.

The characteristics of the H_2 Lyman and Werner band spectra observed in Jovian auroral emissions are significantly affected by methane and acetylene, which absorb differentially over the H_2 band's spectral range. The measure of this differential absorption is the color ratio, which Livengood et al. (1990) have defined as the ratio of the integrated intensities (I) of two wavelength bands: I(1557-1619Å)/I(1230-1300Å).This ratio can be used to infer the methane column density above the region of peak H_2 band emissions: since methane is a strong absorber in the wavelength range 1230 to 1300Å and not in the range 1557 to 1600Å, a high color ratio indicates a large column abundance of methane. The methane absorption effects are related to the H_2 vertical distribution through the specified eddy diffusion coefficient and thermal structure. Electron energies used in the model to determine bremsstrahlung X ray fluxes are chosen by inputting electron beams into the assumed model atmosphere and then selecting the ones that fit to the observed color ratios for CH_4 absorption.

Uncertainty in determining the primary electron beam energy is introduced by assuming that the equatorial and auroral regions of the atmosphere have the same vertical structure. The present uncertainty hinges on our lack of knowledge about the high-latitude methane vertical structure and for the present we simply use the measured near-equatorial structure inferred from Voyager UVS measurements [Festou et al., 1981]. However, we note that if Ulysses determines a bremsstrahlung X ray photon energy spectrum then it will provide an independent constraint on the precipitating electron energy distribution. Simultaneous ultraviolet observations of the color ratio by an ultraviolet observatory (such as HST) would thereby not only allow us to check our modeling assumptions, but would provide unique information on the polar auroral atmosphere.

Anticipated Ulysses GRB Observations

The GRB instrument on Ulysses consists of two hemispherical shell CsI scintillators coupled to phototubes for measuring X rays in the range of 20 to 150 keV, with time resolution up to 8 ms. A detailed description of the instrument can be found in Hurley et al. [1992]. We have calculated the Ulysses sensitivity to Jovian X rays from data accumulated over the first year of operation. During solar quiet periods, which are characteristic of the majority of the mission, the 18-100 keV background rate of each detector is around 200 counts/second; this arises primarily from the diffuse cosmic X ray background and the Radioisotope Thermoelectric Generator aboard the spacecraft. Using the corresponding count rates in the individual energy channels, and assuming a 100 minute integration, we obtain the 3 sigma sensitivities given in Table I and shown in Figure 2.

The closet approach of the Ulysses spacecraft to Jupiter will occur on February 8th of 1992. The spacecraft will approach Jupiter over the north polar cap, pass through perijove near 6.3 R_J, and exit the Jupiter system over the southern polar cap. Although Jupiter's trapped energetic particles will preclude observations near the equator, observations over the north and south poles will be possible before and after closet approach.

Results

Model H_2 band calculations have been matched to the statistical information concerning ultraviolet emission intensity and color ratio determined by ten years of IUE observations [Livengood et al., 1990], and the flux and energy distribution of the incoming electrons have been calculated. These calculated electron beams have been used to compute bremsstrahlung X ray fluxes, which serve as the predictive data set for the Ulysses GRB observations.

The specification of the precipitating electron spectrum is of the form $J(E)=J_{op}(E/E_{op})\ \exp(-E/E_{op})$, where the parameter J_{op} specifies the differential flux (cm^{-2} s^{-1} keV^{-1}) and E_{op} the characteristic energy (keV) of the precipitating electrons. Since the IUE observations show that both the intensity and the color ratio are strong functions of the S_{III} longitude, we have modeled these observations using three independent sets of primary electron parameters which correspond to ultraviolet observational values at 0, 150, and 180 degrees S_{III} longitude in the northern auroral zone (NAZ). The electron beam parameters and the associated ultraviolet characteristics are given in Table II for the three cases. The color ratio has been calculated at two zenith view angles, 0 and 60 degrees. The effect of doubling the hydrocarbon density (60° zenith view angle) results in a 11 to 19% increase in the color ratio due to differential methane absorption, as discussed above. The calculated variance of the color ratio illustrates the sensitivity of the calculation to the view angle of the ultraviolet observation and gives some idea of the sensitivity of the calculation to the chosen model atmosphere. Values of the H_2 band intensity and color ratio for the three cases have also been spline-fit to produce a model curve which can be compared to the Livengood et al. [1990] IUE observations. The results of that fit are shown in Figure 1. In Figure 1(a), auroral H_2 band intensities have been integrated over the restricted spectral range 1557-1619Å (a rough comparison

TABLE I. Ulysses GRB Sensitivities

Channel No.	Energy Channel (keV)	Sensitivity (Photons cm^{-2} s^{-1} eV^{-1})
1	18.1 - 31.1	9.8 x 10^{-7}
2	31.1 - 43.5	1.0 x 10^{-6}
3	43.5 - 56.0	9.3 x 10^{-7}
4	56.0 - 68.4	7.7 x 10^{-7}
5	68.4 - 80.9	6.2 x 10^{-7}

TABLE II. Model Parameters and UV Properties

	S_{III} Longitude (degrees)	E_{op} (keV)	Energy Flux (erg cm^{-2} s^{-1})	H_2 Bands (kR)	Color Ratio (zenith angle)
Case 1	0	20	2.8	21.9	1.98(0°) 2.20(60°)
Case 2	150	37	9.8	83.2	4.17(0°) 4.92(60°)
Case 3	180	45	12.1	105.1	5.43(0°) 6.47(60°)

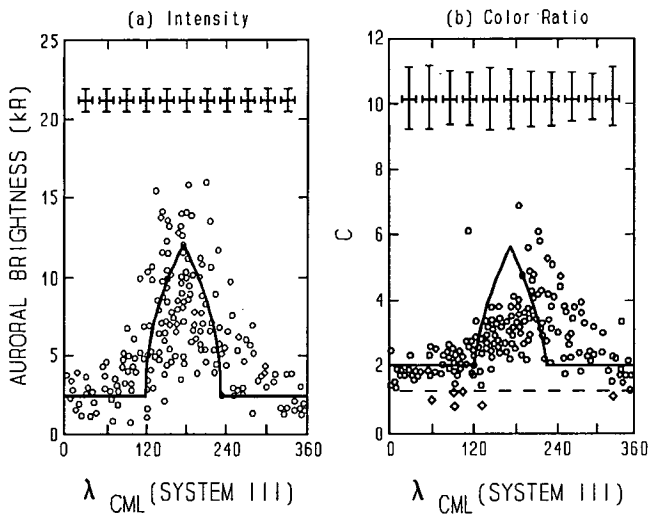

Fig. 1. (a) Intensity and (b) color ratio distribution of the H_2 extreme ultraviolet (EUV) auroral emissions. In Figure 1(a) the H_2 EUV emission intensity in kilorayleighs is integrated over the range 1557-1619 Å. In Figure 1(b) the intensity in the wavelength range 1557-1619 Å has been divided by the intensity in the wavelength range 1230-1300 Å. In (b), the dashed line is the color ratio value for an unattenuated spectrum of H_2 excited by impact of 100-eV electrons; points below this line are plotted as diamonds. The crosses represent the median error bars in longitude and intensity/color ratio for the 60° width centered on each cross. The uncertainty in intensity and color ratio is computed from the camera noise level. The error bars shown here do not include any estimation of possible systematic error as a consequence of erroneous subtraction. The solid lines in both figures are the present model results.

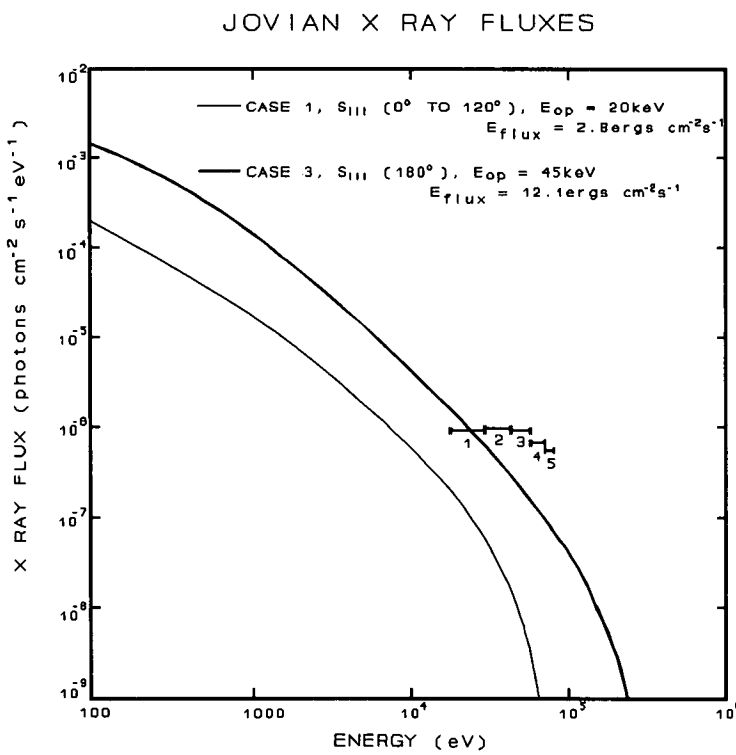

Fig. 2. The X ray intensity as a function of photon energy for a Jovian auroral source size of 5000 by 10,000 km; viewed from a distance of $10R_J$. The solid bars marked 1-5 indicate the 3 sigma sensitivities of the five lower GRB channels for a 100 minute integration.

of this restricted intensity/wavelength integration to the total integrated H_2 Lyman and Werner band intensity given in Table II can be obtained by multiplying by 9.1). The fit appears quite good apart from a phase shift of the color ratio in S_{III} longitude; this could be removed by adjusting the characteristic beam energy, E_{op}, a process not warranted given the present uncertainties of the auroral atmosphere. A likely explanation for this effect is that the time-dependent, atmospheric composition is modified by the precipitating electrons, leading to a characteristic lag in S_{III} longitude of the peak hydrocarbon absorption.

Finally, the X ray fluxes that result from the two extreme electron precipitation cases (case 1: 0 to 120 degrees S_{III} longitude in the NAZ and case 3: 180 degrees S_{III} in the NAZ) are shown in Figure 2. The X ray intensity as a function of photon energy is plotted for an auroral zone emission size 5000 by 10,000 km observed from a distance of 10 R_J. Also plotted on the figure is the sensitivity of several of the GRB energy channels for similar viewing conditions and an integration period of 100 minutes.

Conclusions

The results plotted in Figures 1 and 2 indicate that if the ultraviolet auroral emissions are due to precipitating electrons and the Jovian aurora is sufficiently active (this must be determined by simultaneous EUV observations which will be carried out by the Hubble Space Telescope), then the Ulysses GRB experiment should be able to measure the bremsstrahlung X ray spectrum and place firm constraints on both the precipitating electron flux intensity and energy spectrum. Furthermore, observed S_{III} longitude variations in the spectrum can be used in conjunction with the ultraviolet intensity and color ratio values from HST to determine the vertical hydrocarbon structure in the polar stratosphere of Jupiter. On the other hand, if the major precipitating particles are heavy ions, then GRB would detect nothing since its lowest energy channel at 20 keV is above the threshold for both sulfur and oxygen K-shell emissions.

Acknowledgments. Partial support for this work has been provided by NASA Planetary Atmospheres grant NAGW-1657, NASA IUE and ROSAT Observations of Jupiter's Aurora grant NAG5-1429, and by SwRI Internal Research project 15-9634. The Ulysses project is supported in the United States under JPL Contract 958056 and in Germany by FRG contracts 01 on 088 ZA/WRK275/4-7.12 and 01 on 88014.

References

Ajello, J.M., D. Shemansky, T.L. Kwok, and Y.L. Yung, Studies of Extreme-Ultraviolet Emission from Rydberg Series of H_2 by Electron Impact, Phys. Rev. A., 29, 636-653, 1984.

Broadfoot, S.K., et al., Overview of the Voyager ultraviolet spectrometry results through Jupiter encounter, J. Geophys. Res., 79, 8259-8284, 1981.

Festou, M. C., S. K. Atreya, T. M. Donahue, B. R. Sandel, D. E. Shemansky, and A. L. Broadfoot, Composition and thermal profiles of the Jovian upper atmosphere as determined by the Voyager ultraviolet stellar occultation experiment, J. Geophys. Res., 86, 5715, 1981.

Garvey, R. H., H. S. Porter, and A. E. S. Green, Relativistic yield spectra in H_2, J. Appl. Phys., 48, 4353, 1977.

Gehrels, N., and E. C. Stone, Energetic oxygen and sulfur ions in the Jovian magnetosphere and their contribution to the auroral excitation, J. Geophys. Res., 88, 5537, 1983.

Gladstone, G.R., M. Allen, Y.L. Yung and J.I. Moses, Hydrocarbon photochemistry in the upper atmosphere of Jupiter (abstract), 23rd Annual meeting of the Division of Planetary Sciences of the American Astronomical Society, 4, Palo Alto, CA, November, 1991.

Hurley, K. et al., The Solar X-ray/cosmic-ray burst experiment aboard Ulysses, Astronomy and Astrophysics Suppl., (in press), 1992.

Koch, H. W., and J. W. Motz, Bremsstrahlung cross-section formulas and related data, Rev. Mod. Phys., 31, 920, 1959.

Livengood, T. A., D. F. Strobel, and H. W. Moos, Long-term study of longitudinal dependence in primary particle precipitation in the north Jovian aurora, J. Geophys. Res.,95, 10,375, 1990.

Metzger, A. E., D. A. Gilman, J. L. Luthey, K. C. Hurley, H. W. Schnopper, F. D. Seward, and J. D. Sullivan, The detection of X rays from Jupiter, J. Geophys. Res., 88, 7731, 1983.

Shemansky, D., M. Ajello, and D.T. Hall, Electron Impact Excitation of H_2: Rydberg Band Systems and the Benchmark Dissociative Cross Section for H Lyman-Alpha, Astrophysical Journal, 296, 765, 1985.

Waite, J. H., Jr., T. E. Cravens, J. Kozyra, A. F. Nagy, S. K. Atreya, and R. H. Chen, Electron precipitation and related aeronomy of the Jovian thermosphere and ionosphere, J. Geophys. Res., 88, 6143, 1983.

Waite, J. H., Jr., J. T. Clarke, T. E. Cravens, and C. M. Hammond, The Jovian aurora: Electron or ion precipitation?, J. Geophys. Res., 93, 7244, 1988.

Waite, J.H., Jr., Comment on "Bremsstrahlung X rays from Jovian Auroral electrons" by D.D. Barbosa, J. Geophys. Res., 96 (A11), 19,529, 1991.

Walt, M., L. L. Newkirk, and W. E. Francis, Bremsstrahlung produced by precipitating electrons, J. Geophys. Res., 84, 967, 1979.

D. C. Boice, S. A. Stern, J. H. Waite, Jr., Department of Space Sciences, Southwest Research Institute, P. O. Box 28510, San Antonio, TX 78228.

K. C. Hurley, Space Sciences Laboratory, University of California, Berkeley, Berkeley, CA 94720.

M. Sommer, Max-Planck-Institut für Extraterrestrische Physik, Garching, Germany

(Received November 26, 1991;
accepted December 27, 1991.)

APPENDIX C

The Role of Proton Precipitation in Jovian Aurora: Theory and Observation

J. H. Waite, Jr. [1], D. B. Curran [1], T. E. Cravens [2] and J. T. Clarke [3]

[1] Space Sciences Department
Southwest Research Institute
San Antonio, Texas 78228-0510

[2] Department of Physics and Astronomy
The University of Kansas
Lawrence, Kansas

[3] Department of Atmospheric, Oceanic, and Space Sciences
The University of Michigan
Ann Arbor, Michigan 48109

Abstract

Goertz [1980] proposed that the Jovian auroral emissions observed by Voyager spacecraft could be explained by energetic protons precipitating into the upper atmosphere of Jupiter. Such precipitation of energetic protons results in Doppler-shifted Lyman alpha emission that can be quantitatively analyzed to determine the energy flux and energy distribution of the incoming particle beam. Modeling of the expected emission from a reasonably chosen Voyager energetic proton spectrum can be used in conjunction with International Ultraviolet Explorer (IUE) observations, which show a relative lack of red-shifted Lyman alpha emission, to set upper limits on the amount of proton precipitation taking place in the Jovian aurora. Such calculations indicate that less than 10% of the ultraviolet auroral emissions at Jupiter can be explained by proton precipitation.

Introduction

The first theoretical estimate of the contribution of proton precipitation to Jupiter's aurora was offered by Heaps et al.[1975]. A further theoretical study based on in situ observations of the Voyager plasma and fields experiments suggested the presence of strong proton aurora on Jupiter's night side [Goertz, 1980]. However, since the time of Goertz's original Voyager-inspired analysis, additional evidence has been gathered for the contribution of heavy ion (S^{+q} and O^{+q}) precipitation, both from in situ observations of energetic ion losses in the middle magnetosphere near the Io plasma torus [Gehrels and Stone, 1983] and from inferences about the energy required to produce auroral X rays with the intensity observed by the Einstein X ray telescope [Metzger et al.,1983]. The efforts to establish the identity of the precipitating auroral particles have been complicated yet further by the lack of S and O recombination lines in the FUV H_2 auroral emission spectrum, which suggests that the FUV aurora are largely electron-excited [Waite et al., 1988]. It therefore appears that many different kinds of charged particles may be contributing to the excitation of Jupiter's various auroral emissions.

This paper reports on theoretical calculations of the Lyman alpha line shape expected from proton precipitation impinging on the H_2 atmosphere in the Jovian auroral zone and compares these predictions with high-resolution Lyman alpha line profiles of the Jovian aurora obtained by Clarke et al. [1989] using the International Ultraviolet Explorer. These comparisons are used to determine the role of protons in these auroral emissions. Meinel [1951] used ground-based high-resolution spectroscopy of Doppler-shifted Balmer (H alpha) emission to study the contribution of proton precipitation to the Earth's aurora (cf. Rees, 1989). Similar techniques were applied by Clarke et al. [1989] to study the Jovian aurora using high-resolution Lyman alpha spectra taken with the IUE telescope. No red-shifted Lyman alpha emission with wavelength shifts as expected from energetic protons was observed. However, blue-shifted emissions resulting from fast atomic hydrogen with ten's of eV of translational energy were observed to make up around 50% of the auroral Lyman alpha emission. The lack of significant red-shifted emission suggests that protons are not the primary precipitating particle responsible for the bulk of the observed ultraviolet aurora at Jupiter. On the other hand, the presence of significant blue-shifted emission suggests significant energization and outflow of protons and H atoms and/or significant thermospheric winds as a result of auroral energy dissipation. For further discussion of the blue-shifted emission we refer the reader to Clarke et al. [1989] and Clarke et al. [1991] and for present purposes we concentrate on using the lack of significant red-shifted Lyman alpha emissions to set limits on the energy flux of allowable proton precipitation into the Jovian auroral atmosphere.

The Model

The model employs a continuous slowing-down approximation for an equilibrated beam of energetic hydrogen atoms and protons incident on H_2. The energy loss is given by

$$-\left[\frac{dE}{dz}\right]_{H_2} = n_{H_2}(z)\ L_{H_2}(E)\ \sec(\theta),$$

where $L_{H_2}(E)$ is the total energy loss function in H_2 at energy E, theta is the mean pitch angle of the incoming particles with respect to the vertical, and $n_{H2}(z)$ is the number density of H_2 at altitude z. The energy loss function for protons in H_2 as a function of energy used in the model is that of Anderson and Ziegler [1977].

Two processes for the production of Lyman alpha photons by the interaction of the beam with the H_2 atmosphere are considered:

$$H^+ + H_2 \text{ ---> } H^* + H_2+ \quad (1)$$
$$H + H_2 \text{ ---> } H^* + H_2 \quad (2)$$

Both protons and hydrogen atoms are present in the beam since electron stripping and charge exchange processes between the energetic beam and the H_2 gas are constantly modifying the charge state of the beam (ie., the H^+/H ratio). Due to the energy dependence of these cross sections the beam changes charge state fraction as it dissipates energy in the H_2 atmosphere. The energy-dependent proton-to-hydrogen atom fraction used in this calculation is taken from the work of Allison [1958]. Cross sections for production of Lyman alpha by process (1) at energies below 10 keV are taken from the work of Van Zyl et al.[1990] and above 10 keV from extrapolating using the energy dependence of the ionization cross section as measured by Birely and McNeal [1971].
Cross sections for process (2) are taken from Van Zyl et al. [1990]. Once again a reasonable extrapolation with energy above 10 keV is added on to model processes at higher energies. These cross section values for processes (1) and (2) are shown in Figures 1a and 1b, respectively. An estimate of the beams interaction with the dissociated (atomic) hydrogen component of the suggest that less than 5% of the emission can be attributed to such a source since at the altitude of maximum H^+/H beam energy deposition $n_{H_2} \gg n_H$.

The volume production rates as a function of altitude and energy were calculated by introducing an incident proton/hydrogen beam with a known flux within a specified energy bin. Each beam was then individually tracked as it deposited its energy within the atmosphere. The charge state of the beam (ie., proton to hydrogen ratio) was determined from the beam energy at each altitude step and the volume production rates for processes (1) and (2) were calculated at each altitude during the process of ion beam dissipation using the formulas

$$VP_H.\ (z, E_{init}, E_z) = n_{H_2}(z) \quad f_H^+(E_{init}, E_z) \quad \sigma_{(1)}\ (E_z)$$

$$VP_H\ (z, E_{init}, E_z) = n_{H_2}(z) \quad f_H(E_{init}, E_z) \quad \sigma_{(2)}(E_z)$$

where: VP_i ($i=H^+$ or H) is the volume production at altitude z, initial beam energy E_{init}, and present beam energy at altitude z given by E_z, f_{int} is the $i=H^+$ or H flux from the initial beam of energy E_{init} now at the altitude - dependent energy E_z, and σ_i is the cross section

for Lyman alpha excitation by process i=(1) or (2) at energy E_z. The contribution to the Lyman alpha production as a function of energy and altitude is binned to allow computation of the Doppler-shifted Lyman alpha line profile. The production of Lyman alpha that results from secondary electron production is not included in the present calculation since these emissions are created virtually in the rest frame of the background gas and thus do not contain an observable red-shift.

A precipitating energetic proton spectrum is modeled by taking the Jovian magnetospheric proton spectrum from the Voyager LECP data of Krimigis et al. [1981], scaling it to the desired energy flux, and introducing it into the top of the atmosphere (see Figure 2). The model H_2 atmosphere was taken from the earlier auroral electron modeling of Waite et al.[1983] and is shown for reference in Figure 3. Also shown in Figure 3 is the approximate altitude range for the Lyman alpha emission source and an approximate indication of the methane homopause below which CH_4 absorption of Lyman alpha could affect the results. The beam flux has been normalized to produce an integrated energy flux of 20 ergs cm^{-2} $s^{-1,}$ which is approximately the flux that would be required to produce the observed H_2 Lyman and Werner band systems, UV emissions [Horanyi et al.,1988]. A mean angle of 30° between the magnetic field direction and the IUE view direction was adopted for the observational viewing geometry. The broadening of the line emission from the "actual" pitch angle distributions of the ions (and charge exchanged neutrals) were not accounted for, but were not expected to add considerable broadening beyond the effects brought on by the assumed initial beam energy distribution and subsequent energy decay within the upper atmosphere which are properly accounted for by these calculations.

Results and Conclusions

Red-shifted emission intensities that results from a proton distribution with a total energy flux of 20 ergs cm^{-2} s^{-1} are shown in Figure 4 along with representative IUE Lyman alpha spectra from Clarke et al. [1991]. The location of the peak of the red-shifted Lyman alpha emission is determined by the convolution of the energy dependence of the Lyman alpha production cross sections at low proton/hydrogen energies and the tail at longer wavelengths (above 1220Å) is directly related to the initial beam distribution. The location and shape of the red-shifted Lyman alpha peak from our calculations has been compared to similar observations of terrestrial Lyman alpha from the auroral zone [Ishimoto et al., 1989[and has been shown to be consistent with their results. Not shown in this figure is a 15-30kR Lyman alpha emission at line center (1215.7Å) which would result from secondary electrons produced by the beam atmosphere interaction impinging on atmospheric H and H_2. These secondary electron-generated emissions were not explicitly calculated since they result in no "red-shifted" emission. Such emissions would be easily observable by the IUE telescope. Clarke et al. [1989] did not, however, observe such emission intensities at these wavelengths. Clearly, therefore the observed aurora does not contain a proton energy flux large enough to produce the observed H_2 Lyman and Werner bands. However, a smaller flux of protons is possible given the constraints of the IUE Lyman alpha line profiles. The upper limits of proton precipitation allowed by the observations can be calculated by retaining the same form of the proton energy distribution

as described above and by scaling down the energy flux to match the levels of red-shifted emission seen in the observations. Comparison of the observations with the model line profile suggest that protons comprise 5% or less of the particles responsible for the bulk of the Jovian ultraviolet aurora [cf., Broadfoot et al., 1981]. We note, however, that these results are weakly dependent on the energy spectrum of the precipitating protons. Given the present available data and the model, it is difficult to envision a scenario where protons would be responsible for over 10% of the observed auroral ultraviolet emission. More energetic proton beams (>> 1 Mev) that deposit the bulk of their energy below the hydrocarbon absorption layer are not ruled out by the present observations, but they also cannot contribute to H_2 band ultraviolet auroral emissions.

The results reported here set useful constraints on magnetospheric processes responsible for auroral particle precipitation and add yet a further piece to the ongoing puzzle as to the identity of the particles responsible for Jovian auroral observations. Perhaps in situ confirmation of these results will be possible during the high-latitude encounter of Ulysses with Jupiter in January-February of 1992. In addition, high-resolution spectra at Lyman alpha by HST may provide additional observational constraints on auroral proton precipitation.

References

Allison, S.K.; Experimental Results on Charge-Changing Collisions of Hydrogen and Helium Atoms and Ions at Kinetic Energies Above. 2keV Reviews of Mod Phys., vol. 30, p. 1137, 1958.

Anderson & Ziegler, Stopping and Ranges of Ions in Matter, vol. 3: Hydrogen Stopping Powers and Ranges in all Elements, Pergamon Press. 1977.

Birely, J.H., McNeal, R.J. "Lyman Alpha Emission Cross Sections for Collisions of H_t and H with N_2 and O_2. *JGR*, **76**, 3700, 1971.

Broadfoot, A.L., et al., Overview of the Voyager ultraviolet spectrometry results through Jupiter encounter, *J. Geophys. Res.*, **86**, 8259-8284, 1981.

Clarke, J. T., J. Trauger, and J.H. Waite, "Doppler shifted H Ly α emission from Jupiter's aurora", *Geo. Res. Lett., 6*, 587, 1989.

Clarke, J.T., G.R. Gladstone, and L. Ben-Jaffel, Dayglow H Lyman alpha emission profile, *Geophys Res. Lett.*, **18**, 19, 1991.

Gehrels, N. and E.C. Stone, "Energetic oxygen and sulfur ions in the Jovian magnetosphere and their contribution to the auroral excitation, *J. Geophys. Res.*, **88**, 5537, 1983.

Goertz, C.K., "Proton aurora on Jupiter's nightside", *Geo. Res. Lett., 7*, 365, 1980.

Heaps, M.G., B.C. Edgar, and A.E.S. Green, "Jovian proton aurora". *Icarus*, **24**, 78, 1975.

Horanyi, M., T.E. Cravens, and J.H. Waite, Jr., The precipitation of energetic heavy ions into the upper atmosphere of Jupiter, *J. Geophys. Res.*, **93**, 7251-7271, 1988.

Ishimoto, M., C.-I. Meng, G.R. Romick, and R.W. Huffman, Doppler shift of auroral Lyman α observed from a satellite, *Geophys. Res. Lett.*, **16(2)**, 143, 1989.

Krimigis, S.M., J.F. Carbary, E. P . Keath, C.O. Bostrom, W.I. Axford, G. Gloeckler, L.J. Lanzerotti, and T.P. Armstrong, "Characteristics of hot plasma in the Jovian magnetosphere: Results from the Voyager Spacecraft", *J. Geophys. Res., 86*, 8227, 1981.

Meinel, A.B., "Doppler-shifted auroral hydrogen emission", *Astrophys. J.*, **113**, 50, 1951.

Metzger, A., et al., "The detection of X-rays from Jupiter", *J. Geophys. Res.*, **88**, 7731, 1983.

Rees, M.H., Physics and chemistry of the upper atmosphere, pages 45-52, Cambridge University Press, Cambridge, U.K., 1989.

Van Zyl, B., M.W. Gealy, and H. Neumann, Lyman-α emission from low-energy H + H_2 and H^+ + H_2 collisions, accepted for publication in *Phys. Rev. A.*, 1990.

Waite, J.H., T.E. Cravens, J. Kozyra, A.F. Nagy, S.K. Atreya, and R.H. Chen, "Electron precipitation and related aeronomy of the Jovian thermosphere and ionosphere", *J. Geophys. Res., 88*, 6143, 1983.

Waite, J.H., J.T. Clarke, T.E. Cravens, and C.M. Hammond, "The Jovian aurora: electron or ion precipitation?", *J. Geophys. Res.*, **93**, 7244, 1988.

Figure Captions

Figure 1: Cross sections for Lyman alpha excitation of a) protons on H_2 and b) hydrogen atoms on H_2 taken from the work of Van Zyl et al.[1990].

Figure 2: Detailed spectral fit to the low-energy ion channels. Plotted (closed circles) are the intensities measured in sector f (~90° from convection direction) of the PL02-PL07 channels. In this direction, the detector response is thought to be due to protons only. The dotted curve shows the thermal distribution obtained using parameters listed in the figure. The dashed curve indicates a power law fit with a spectral index of 2.8. The closed square is from the LEPT detector channel which is sensitive only to protons. [Krimigis et al., 1981].

Figure 3: H_2 model atmosphere altitude profile from Waite et al.[1983]. Also indicated on the figure are the altitude of the doppler shifted Lyman alpha emission and the approximate altitude of the methane homopause below which altitude Lyman alpha absorption by methane could significantly affect our results.

Figure 4: The brightness numbers as a function of wavelength for both the model and the IUE SWP spectra (December, 1986). The brightness numbers assume that the emitting region is an auroral zone which is diffuse East-West (i.e. fills the 9 arc second large aperture) and is less than the IUE spatial resolution of 5 arc seconds North/South (i.e. is unresolved). Figure 4(a) shows the IUE SWP 29880 spectra data compared to a proton aurora energy flux of 20 ergs $cm^{-2}s^{-1}$ which is roughly that required to account for the H_2 Lyman and Werner band emissions that were observed. Figure 4(b) shows a comparison of new IUE SWP spectra 44340 and 44342 with a 5% intensity of the 20 erg $cm^{-2}s^{-1}$ aurora (1.0 ergs $cm^{-2}s^{-1}$) to illustrate the emission allowed by the present observations.

Acknowledgements

Partial support for this work has been provided by NASA Planetary Atmospheres grant NAGW-1657, NASA IUE and ROSAT Observations of Jupiter's Auroral grant NAG5-1429, and by SwRI Internal Research project 15-9634.

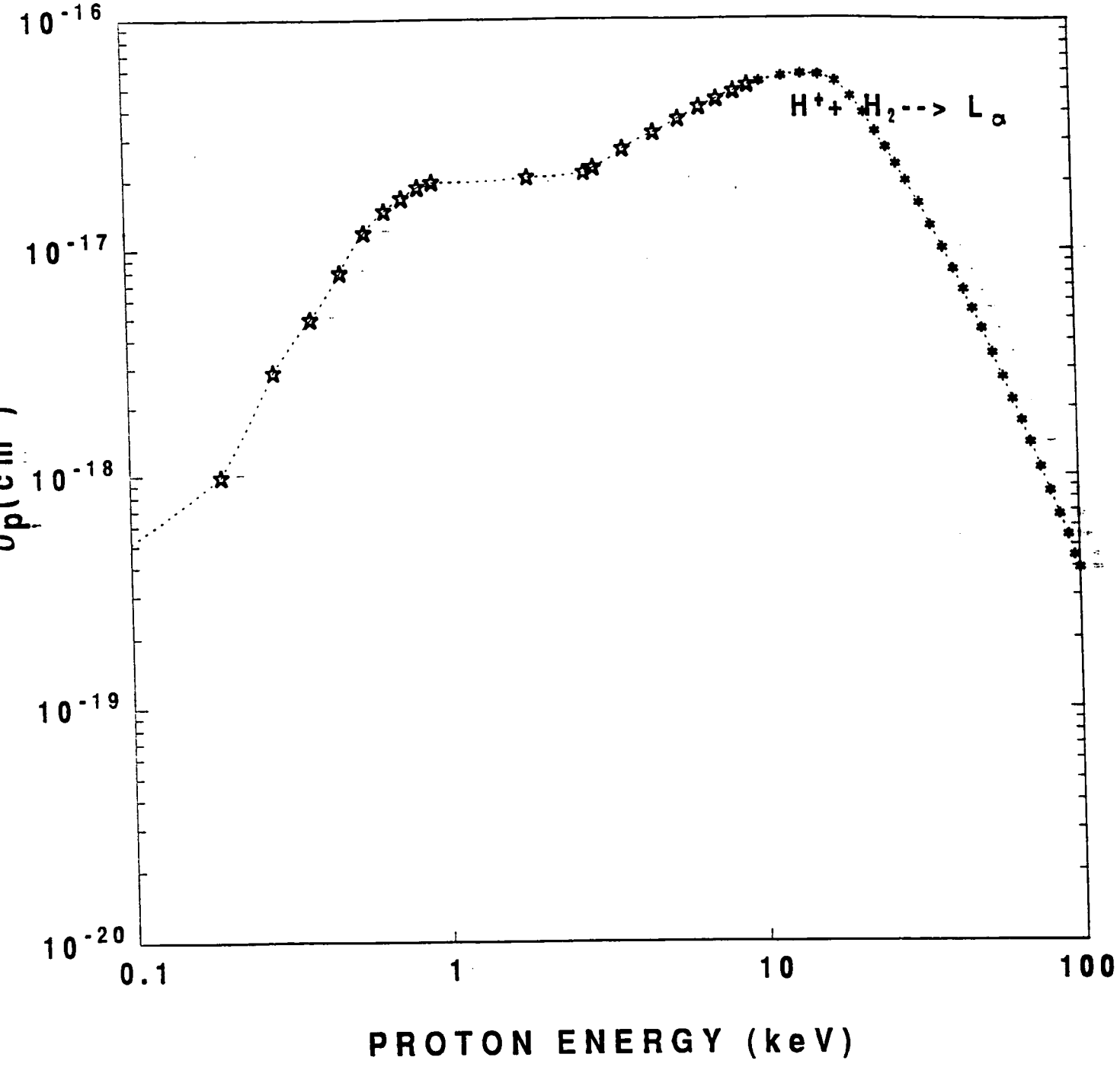

Figure 1a

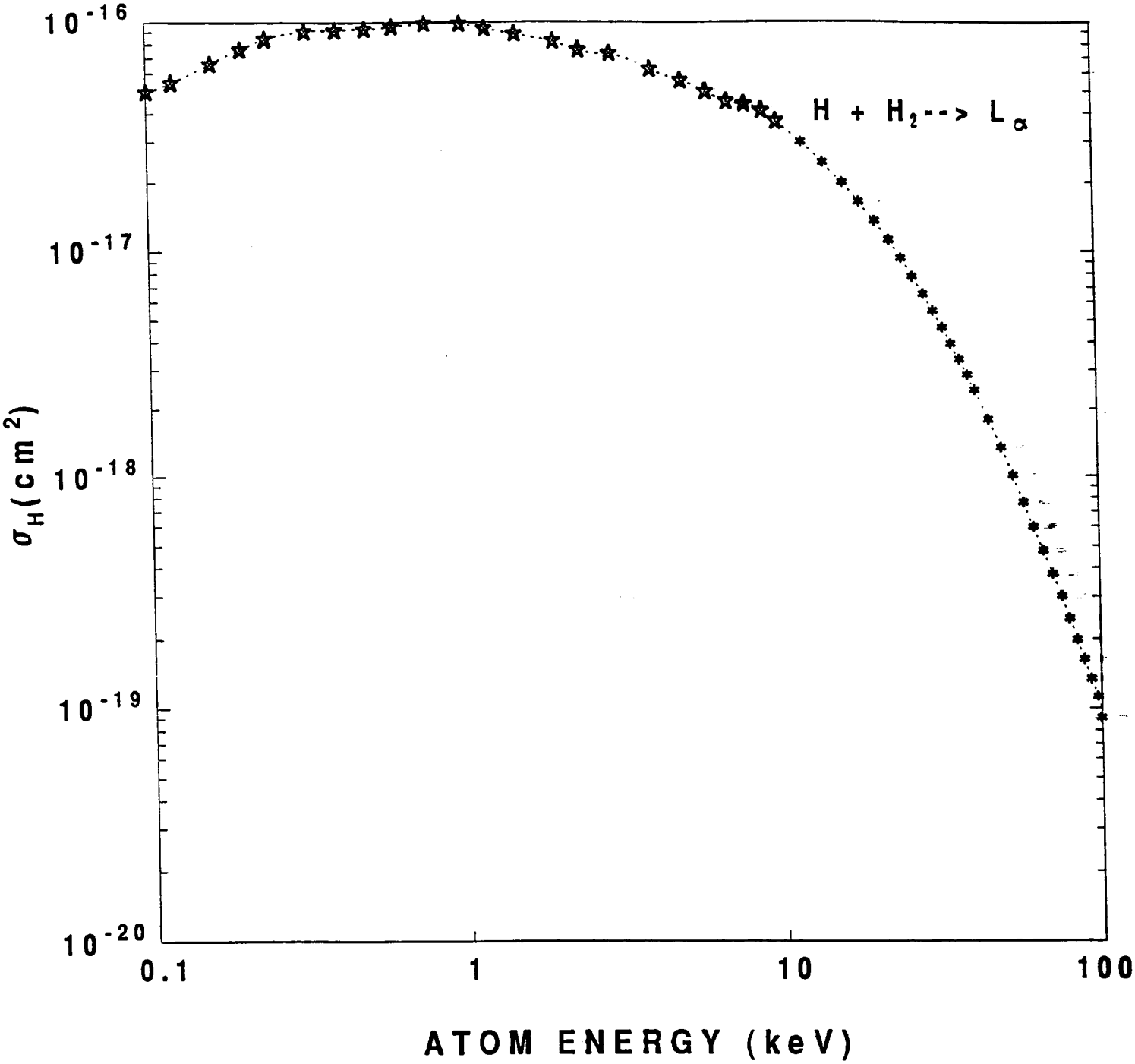
10^{-16}
10^{-17}
10^{-18}
10^{-19}
10^{-20}
$\sigma_H(cm^2)$
$H + H_2 \rightarrow L_\alpha$
0.1
1
10
100
ATOM ENERGY (keV)

Figure 1b

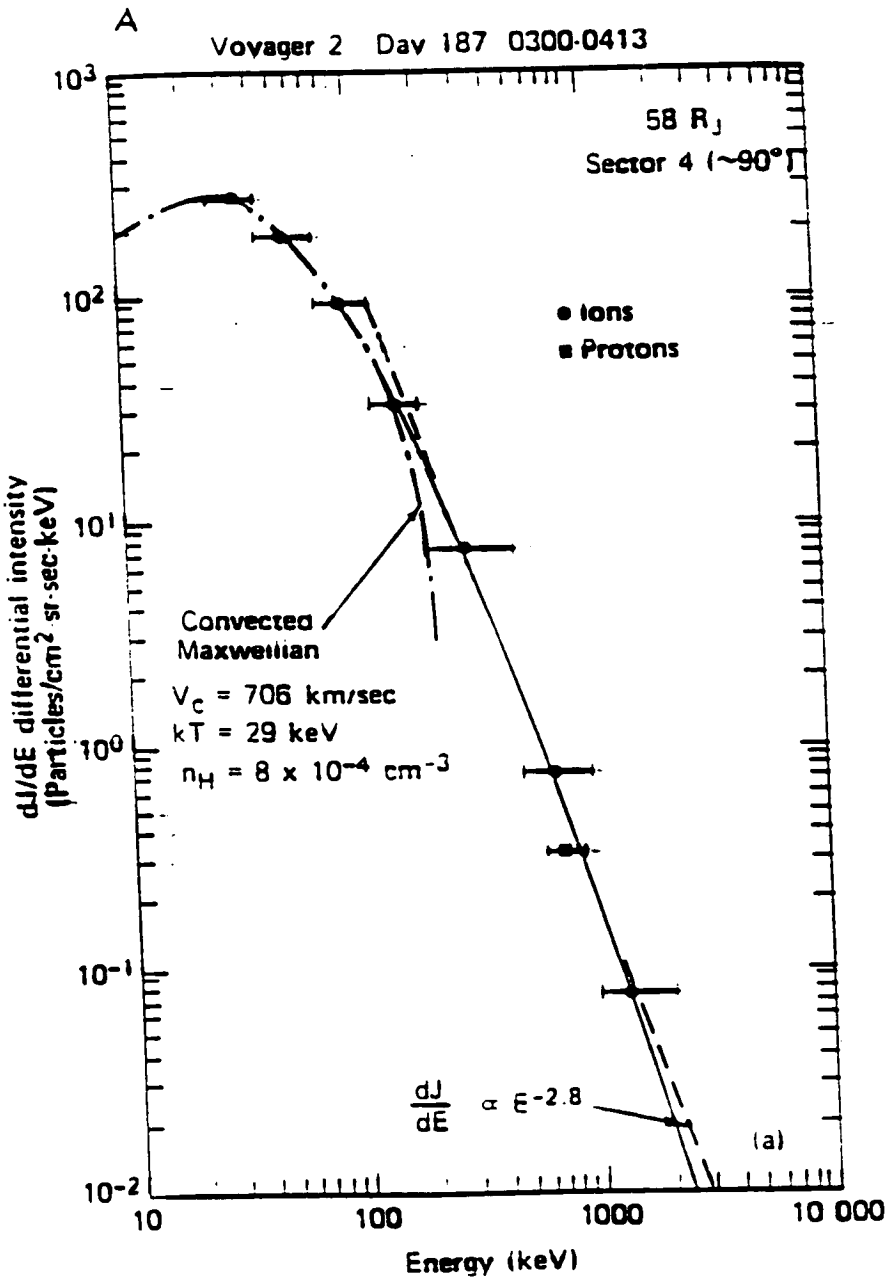
A
Voyager 2 Day 187 0300-0413
58 R_J
Sector 4 (~90°)
● Ions
■ Protons
Convected Maxwellian
V_c = 706 km/sec
kT = 29 keV
$n_H = 8 \times 10^{-4}$ cm^{-3}
$\frac{dJ}{dE} \propto E^{-2.8}$
(a)
dJ/dE differential intensity (Particles/cm^2 sr sec keV)
Energy (keV)
10^3
10^2
10^1
10^0
10^{-1}
10^{-2}
10
100
1000
10 000

Figure 2

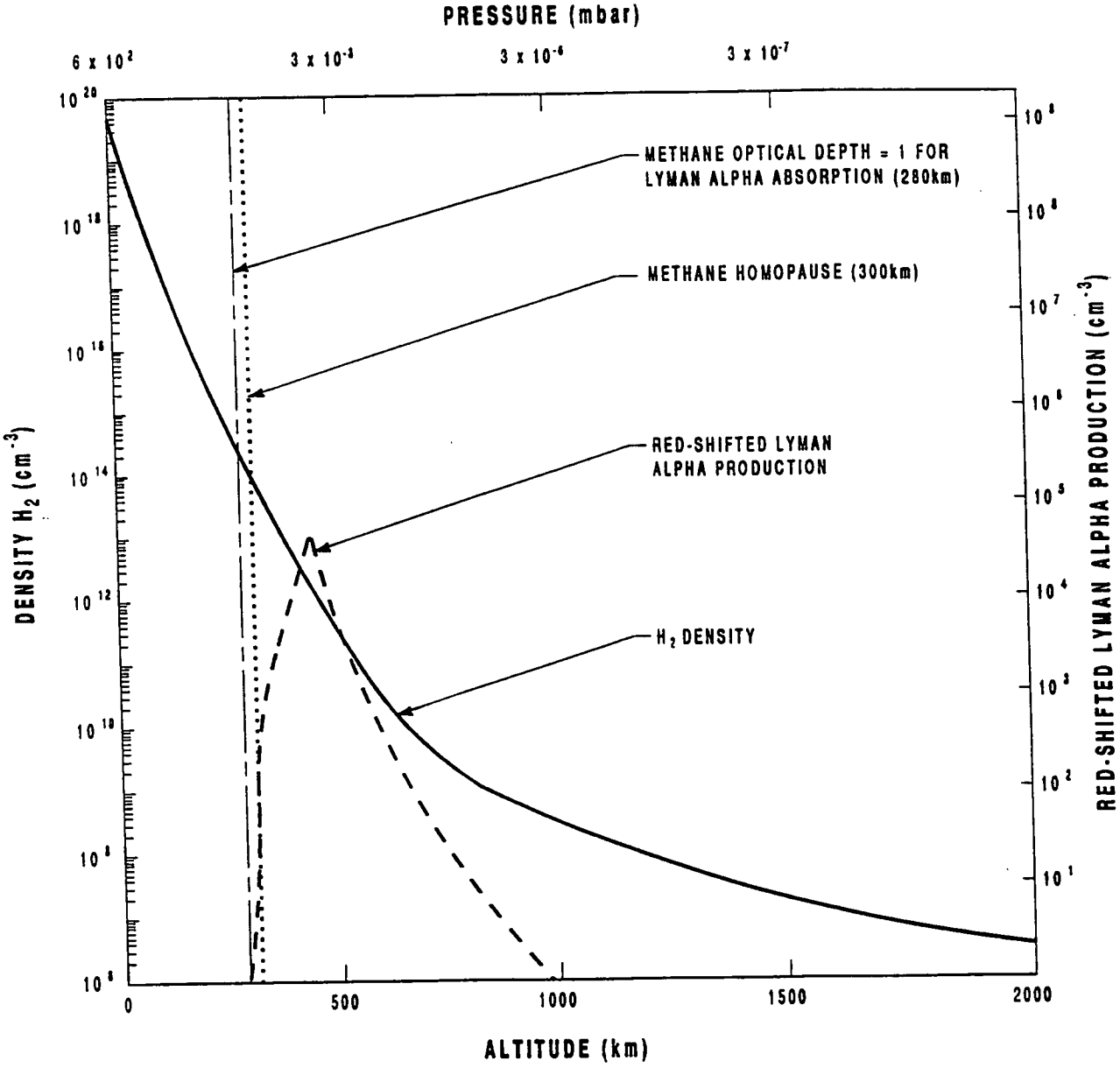
PRESSURE (mbar)
6 x 10⁻²
3 x 10⁻⁴
3 x 10⁻⁶
3 x 10⁻⁷
METHANE OPTICAL DEPTH = 1 FOR LYMAN ALPHA ABSORPTION (280km)
METHANE HOMOPAUSE (300km)
RED-SHIFTED LYMAN ALPHA PRODUCTION
H₂ DENSITY
DENSITY H₂ (cm⁻³)
RED-SHIFTED LYMAN ALPHA PRODUCTION (cm⁻³)
ALTITUDE (km)
0
500
1000
1500
2000

Figure 3

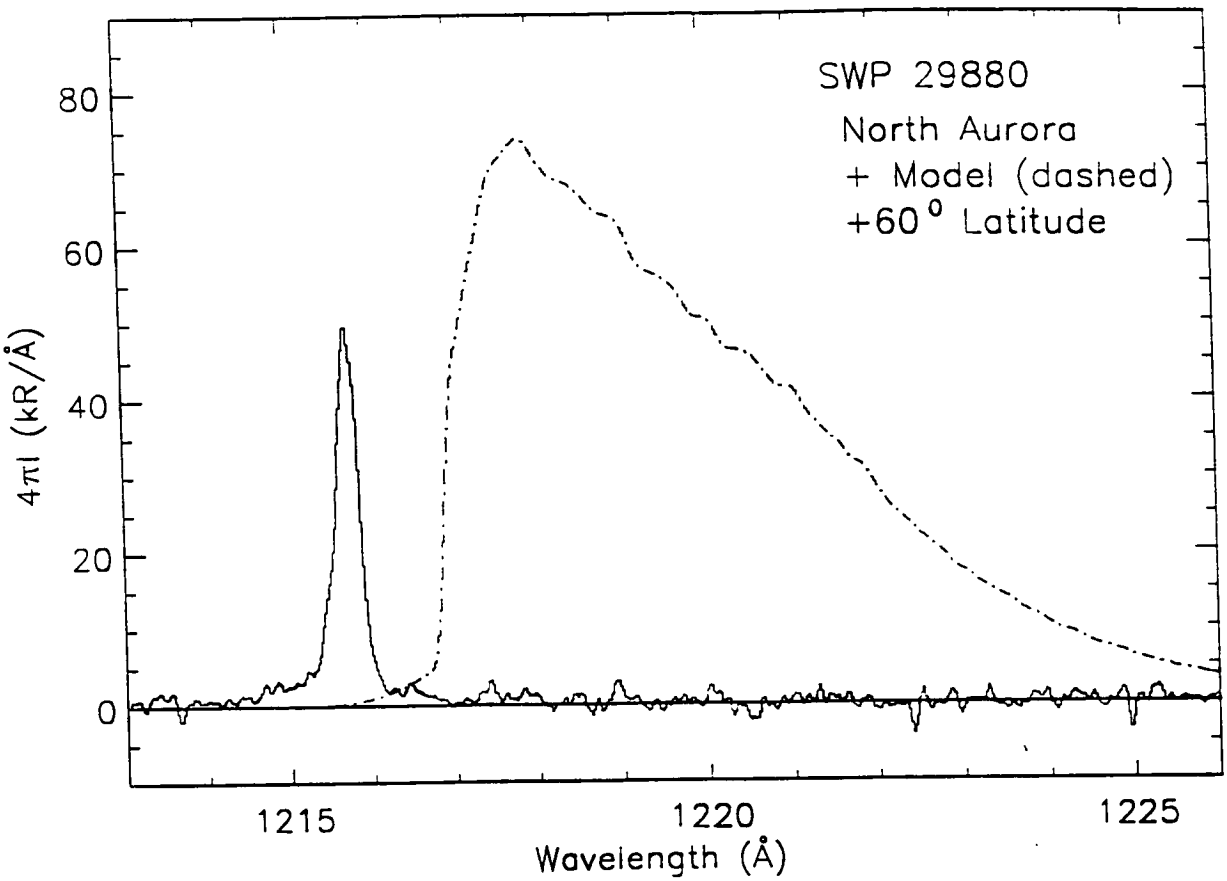
SWP 29880
North Aurora
+ Model (dashed)
+60° Latitude
80
60
40
20
0
4πI (kR/Å)
1215
1220
1225
Wavelength (Å)

Figure 4(a)

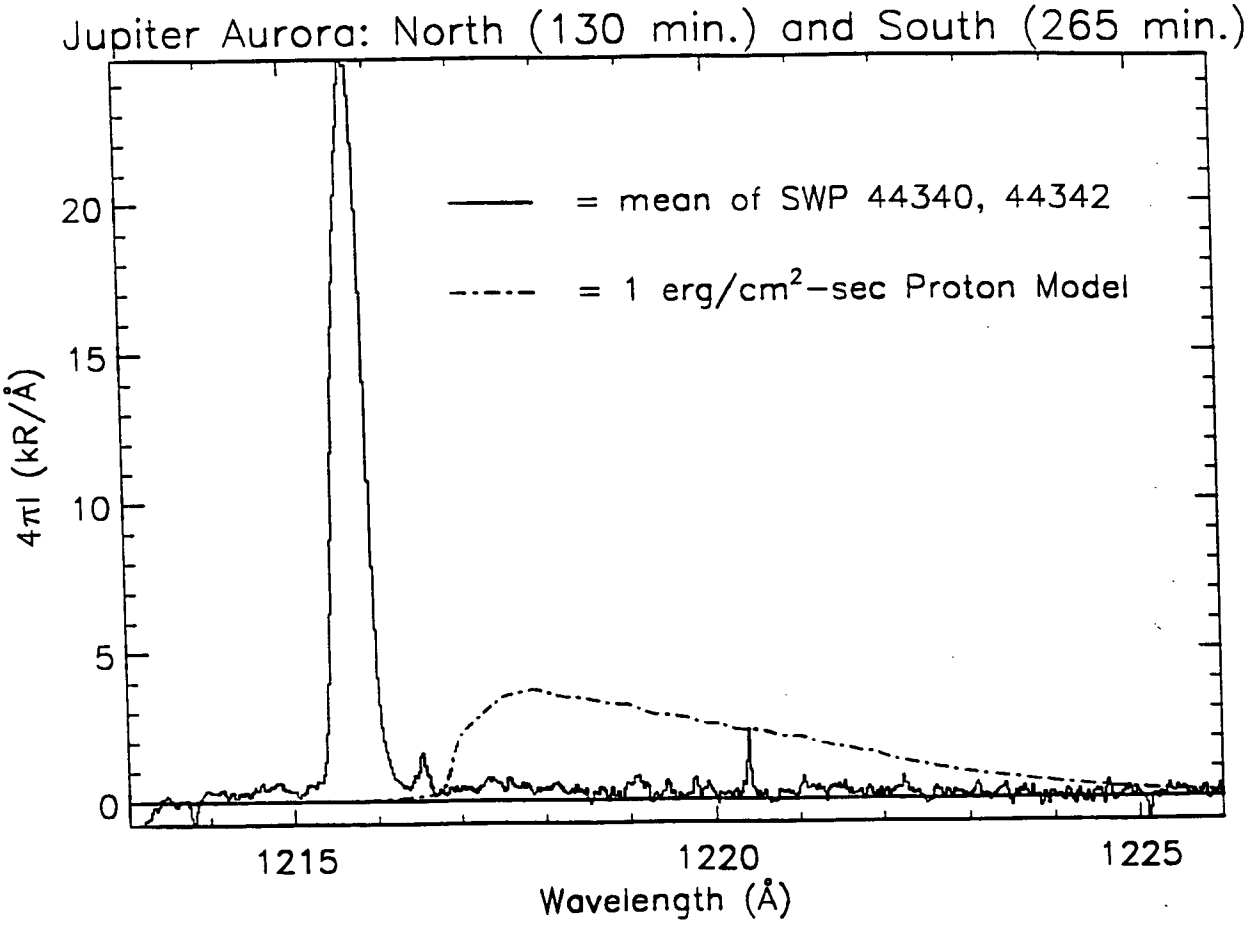
Jupiter Aurora: North (130 min.) and South (265 min.)
= mean of SWP 44340, 44342
= 1 erg/cm²−sec Proton Model
4πI (kR/Å)
0
5
10
15
20
1215
1220
1225
Wavelength (Å)

Figure 4(b)

APPENDIX D

Lyman Alpha Line Shapes from Electron Impact H_2 Dissociative Processes in the Jovian Auroral Zone

J. H. Waite, Jr.[1] and G. R. Gladstone[2]

[1]Space Sciences Department
Southwest Research Institute
San Antonio, Texas 78228-0510

[2]Space Physics Laboratory
University of California, Berkeley
Berkeley, California

Introduction

Over the past two years several Lyman alpha line profile spectra of Jupiter have been obtained using the International Ultraviolet Explorer (IUE) telescope facility. Several different regions of the planet have been observed including the auroral zone [Clarke et al.,1989], the low and mid latitudes [Clarke and Gladstone, 1990], and the equatorial region which includes the Lyman alpha bulge region [Clarke et al., 1991]. These results have presented a very interesting, but yet understood picture of atomic hydrogen at Jupiter with explanations that range from ion outflow in the auroral zone to large thermospheric winds at low and mid latitudes. New data are needed to address the outstanding questions. Almost certainly, high resolution spectra from the Hubble Space Telescope will play a role in new observations. Better data also require better models and better models new laboratory data as inputs. The purpose of this letter is two-fold: 1) to introduce a method by which the new laboratory electron impact measurements of H_2 dissociation of Ajello et al. [1991] can be used to calculate both the slow and fast $H(^2S)$ and $H(^2P)$ fragments in an H_2 atmosphere, and 2) to determine the predicted Lyman alpha line shape that would result from electron impact production of these dissociative fragments in the Jovian auroral zone.

Determination of Electron Impact Produced H_2 Dissociative Products

The calculation of fast and slow $H(^2S)$ and $H(^2P)$ rely heavily on the new cross section presented in Ajello et al. [1991]. In this letter, we reproduce Table 1 and Table of the Ajello et al. paper as reference and provide a cook book method for using that information to construct production rates for fast and slow $H(^2S)$ and $H(^2P)$ production from electron impact on H_2.

1. Slow $H(^2P)$ production due to singlet and triplet H_2 excitation is found by simply adding together the fit parameters from Table 1 [Ajello et al., 1991] for processes 1, 2, and 3.

2. Slow $H(^2S)$ production was calculated using the derived values of $H(^2P)/H(2l)$ for energies above 50ev of 59% from the Ajello et al., [1991] experiment.

3. Fast $H(^2P)$ production due to doubly excited states is found in a similar manner by adding the cross sections from processes 4, 5, and 6 of Table 1 of Ajello et al. together.

4. Values found in Table 2 of the Ajello et al. reference were then used to deduce a value of for the $H(^2S)$ relative to the $H(^2P)$ production for fast $H(^2S)$ production. The number is 0.82.

The Model and Results

The results of the above determination of electron impact produced H_2 dissociative products provides production rates for fast and slow $H(^2S)$ and $H(^2P)$ when included in the context of an electron transport calculation of the auroral energy dissipation. This was accomplished by inclusion of the H_2 dissociative production rates in the two -stream electron transport equation which has been used in the past to model Jovian electron aurora (cf., Waite et al., 1983). The precipitating electron energy spectrum was specified by the equation:

$$J(E) = J_{op}\,(E/E_{op})\,e^{-E/Eop} \quad \text{where } E_{op} = 100 \text{ keV and } J = 10^6 \text{ cm}^{-2}\text{ s}^{-1}\text{ keV}^{-1}.$$

This results in an integrated electron energy influx of 10 ergs cm^{-2} s^{-1} which is sufficient to explain the bulk of the H_2 Lyman and Werner band emissions observed in the Jovian aurora if the particles are indeed electrons. The resulting production rate profiles for the fast and slow H^*, H_2 Lyman and Werner band, and direct excitation of atomic hydrogen by electron impact as a function of altitude are presented in Figure 1.

These production rate profiles were then used as inputs into the radiative transfer model of Gladstone [1982] to produce a Lyman alpha line profile as viewed from the top of the atmosphere. The line profile is shown in Figure 2 where we have labeled the various contributions independently: 1) e + H_2(slow) is the solid line, 2) e+ H_2(fast) is the dotted line, and 3) e + H is the dashed line. Here we have assumed that all $H(^2S)$ is rapidly turned into $H(^2P)$ by collisions with H_2, a good assumption for the energetic electron beams chosen which deposit their energy near the homopause at a pressure level of 0.1 millibars.

Conclusions

Although the line broadening produced from including fast H_2 dissociative fragments from electron impact cannot explain the highly broadened features indicative of the present data sets, high temporal, spatial, and spectral resolution data from HST must include these processes in future quantitative models. Inclusion of this data in future models will allow quantitative estimates of winds and atmospheric turbulence to be determined from this high resolution data. Such an understanding of the atmospheric dynamics of the Jovian auroral zone is crucial to determination of the global structure of the Jovian thermosphere due to the dominance of the auroral energy input over solar EUV processes (> a factor of 10, cf. Waite et al., 1983).

Acknowledgements

Partial support for this work has been provided by NASA Planetary Atmospheres grant NAGW-1657, NASA IUE and ROSAT Observations of Jupiter's Aurora grant NAG5-1429, and by SwRI Internal Research project 15-9634.

References

Ajello, J.M., D.e. Shemansky, and G.K. James, "Cross sections for production of H(2p, 2s, 1s) by electron collisional dissociation of H_2, *The Astrophysical Journal, 371*, 422, 1991.

Clarke, J.T., J. Trauger, and J.H. Waite, "Doppler shifted H Ly α emission from Jupiter's aurora", *Geo. Res. Lett., 6*, 587, 1989.

Clarke, J.T. and G.R. Gladstone, The center to limb variation in Jupiter's H Ly-α emission, submitted to *J. Geophys. Res. Brief Rpts.*, 1990.

Clarke, J.T., G.R. Gladstone, and L. Ben Jaffel, "Jupiter's Line Profiles", *Geophys. Res. Lett.*, in press, 1991.

Gladstone, G.R., "Radiative transfer with partial frequency redistribution in inhomogeneous atmospheres: application to Jovian aurora, *J. Quant. Spectrae. Radiat. Transfer, 27*, 545-556, 1982.

Waite, J.H., T.E. Cravens, J. Kozyra, A.F. Nagy, S.K. Atreya, and R.H. Chen, "Electron precipitation and related aeronomy of the Jovian thermosphere and ionosphere", *J. Geophys. Res., 88*, 6143, 1983.

Figure Captions

Figure 1: Lyman alpha production rates from all electron impact processes on H_2 and H as a function of altitude for the 100 keV auroral case.

Figure 2: Lyman alpha line profile, intensity in kilo Rayleighs per angstrom as a function of relative wavelength from line center.

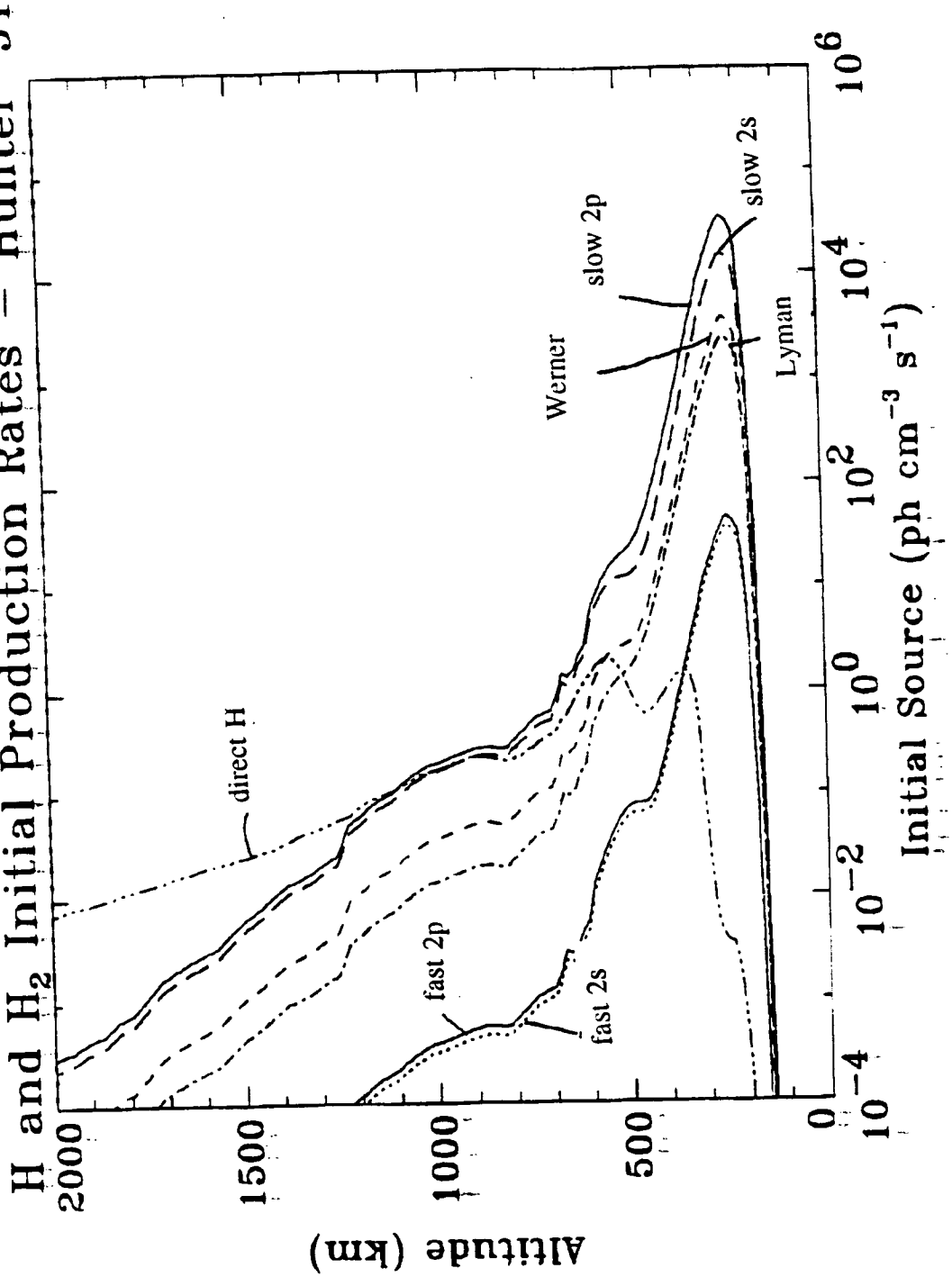
H and H2 Initial Production Rates – Hunter '91
Altitude (km)
2000
1500
1000
500
0
Initial Source (ph cm-3 s-1)
10-4
10-2
100
102
104
106
direct H
fast 2p
fast 2s
Werner
slow 2p
slow 2s
Lyman

Figure 1

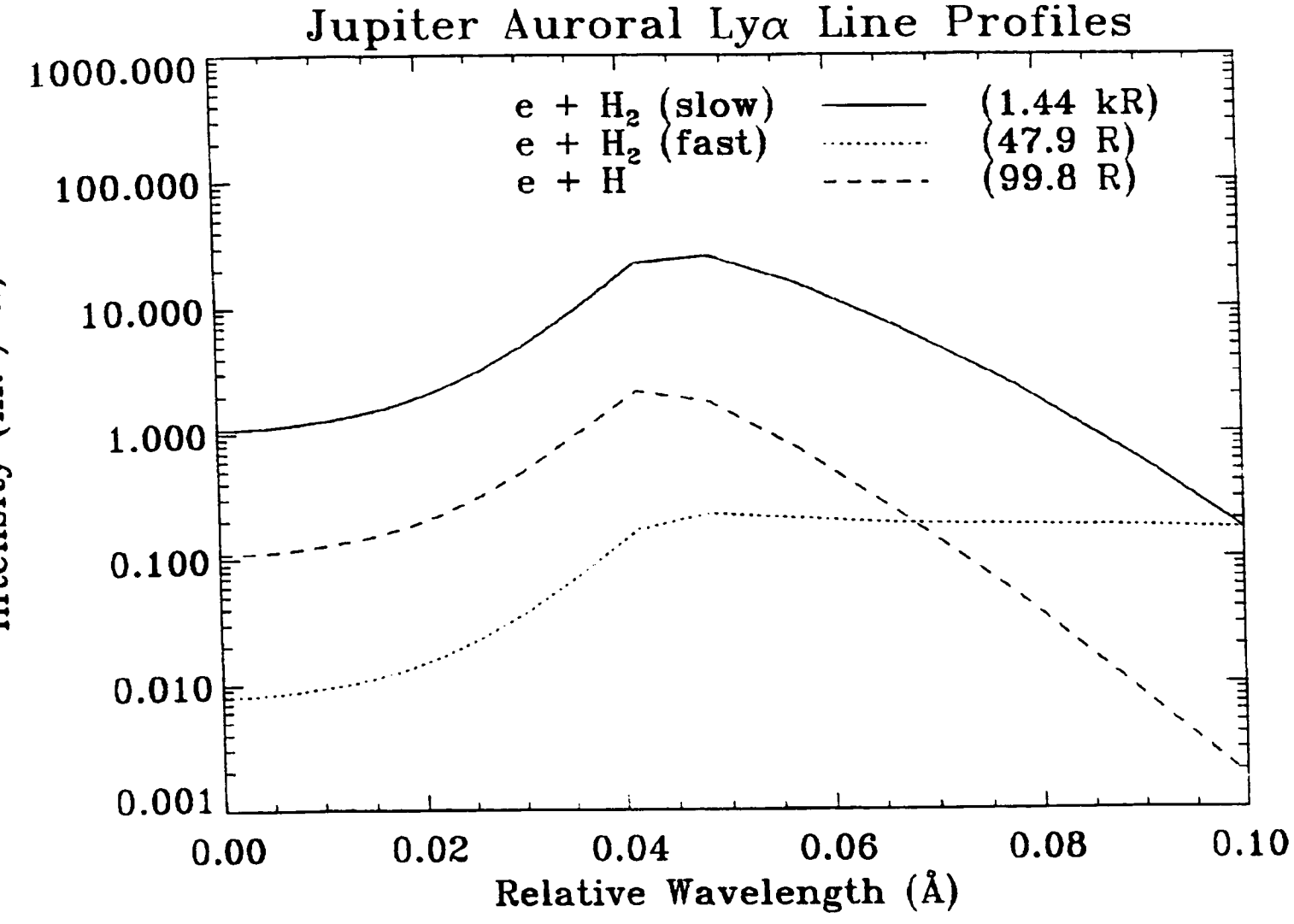
Jupiter Auroral Lyα Line Profiles
1000.000
100.000
10.000
1.000
0.100
0.010
0.001
e + H2 (slow)
e + H2 (fast)
e + H
(1.44 kR)
(47.9 R)
(99.8 R)
0.00
0.02
0.04
0.06
0.08
0.10
Relative Wavelength (Å)

Figure 2

APPENDIX E

Multispectral Observations of the Jovian Aurora

Introduction

The upper atmospheres of the Earth and the outer planets form a screen on which precipitating charged particles, like the electron beam in a television, trace fleeting, but revealing patterns of visible, ultraviolet, infrared, and x ray emissions that offer valuable clues to processes occurring within the planetary magnetospheres. At Earth, years of in situ measurements, as well as ground based observations, have yielded a picture (still fuzzy) where the interaction of the solar wind with the magnetosphere of the Earth provides a complex path for the storage and release of energy during magnetic substorms; the ultimate manifestation of terrestrial auroral processes. More recent global imaging of substorm events from high above the Earth (> 3.5 R_e) by Dynamics Explorer have made a unique contribution towards understanding the global and temporal evolution of such auroral events by providing a morphological perspective and by providing the crucial observational link that allows the separation of spatial and temporal variations inherent in the interpretation of in situ data. A similar role was played by the Hubble Space Telescope (HST) during the recent encounter of Ulysses with Jupiter February, 1992 in helping to define a new paradigm in Jovian auroral physics. The old paradigm portrayed Jupiter's magnetosphere as totally dominated by internal processes (ie. Io related tori, heavy ions, etc.) where energetic heavy ion precipitation in the inner magnetosphere was solely responsible for the observed auroral phenomena. Ulysses and HST portray a more Earth-like paradigm where electron acceleration in the outer magnetosphere near the boundary with the solar wind plays a distinct role in the formation of auroral hot spots, yet energetic heavy ions also enter into the picture [this paper; Dols et al., 1992] (similar to the role of the energetic ions from the terrestrial ring current during magnetic substorms). These heavy ions as a result of excitation during their transit through the atmosphere produce the x ray emissions observed in Roentgensatellit (ROSAT) x ray energy spectra.

The ultraviolet spectrometers on the Voyager 1 and 2 spacecraft [Sandel et al., 1979; Broadfoot et al., 1981] and the International Ultraviolet Explorer (IUE) spacecraft [Clarke et al., 1980; Yung et al., 1982] observed intense H_2 Lyman and Werner band emissions from the Jovian atmosphere at high latitudes, thus providing evidence for auroral particle precipitation at Jupiter. Observations in the infrared [Caldwell et al., 1980; 1983] showed spatial dependencies similar to those at ultraviolet wavelengths. X ray emissions were seen by the High Energy Astronomical Observatory 2 (Einstein) in the Jovian auroral zone [Metzger et al., 1983]. Taken together, these observations provide indications of an aurora more than 100 times more powerful ($>10^{13}$ Watts) than Earth's, which has a strong influence on the high-latitude structure, dynamics, and energetics of the upper atmosphere of Jupiter.

Earlier observations of the Jovian x ray aurora [Metzger et al., 1983] and in situ measurements of energetic oxygen and sulfur [Gehrels and Stone, 1983] indicated that energetic sulfur and oxygen were precipitating into the high-latitude Jovian atmosphere and were largely responsible for the observed ultraviolet auroral emissions. Building on the earlier work concerning electron aurora [Waite et al., 1983], Horanyi et al. [1988] developed a quantitative

model of the interaction of energetic oxygen ions and atoms with an H_2, H atmosphere. The model results indicated that sulfur and oxygen emissions in the ultraviolet at 1256 and 1304 angstroms should be detectable with the IUE UV telescope. Subsequent observations and analysis, however, showed no detectable emission at 1304 angstroms and an uncertain detection at 1256 angstroms [Waite et al., 1988]. This lead Waite and colleagues to conclude that the bulk of the observable UV auroral emissions are probably due to electrons and that the ions that do precipitate are quite energetic (>300 KeV/nucleon) and are responsible for the x ray emissions, but do not make a significant contribution to the ultraviolet auroral emissions.

The conclusion of Waite et al. [1988] was not readily endorsed by the Jupiter magnetospheric community, which continued to embrace the dominant role of heavy ion precipitation as a source for the Jovian aurora. Until recently little new observational information was available to allow a re-examination of the energetic ion paradigm. However, the recent Ulysses encounter with Jupiter and the coordinated HST auroral imaging campaign reported in this paper present new evidence for an expanded role for electrons and association of the energetic electron source with the Jovian magnetopause boundary. In addition, ROSAT observations confirm the role of energetic heavy ions in x ray production, but suggest that the source is limited to energies greater than 300 KeV/ nucleon and as suggested by Waite et al. [1988] comprises only a fraction of the measured ultraviolet emission. Thus, a new paradigm of Earth-like auroral processes appears to be emerging from these exciting new results.

Hubble Space Telescope Faint Object Camera Images: Observations and Analysis

Three separate HST investigations were scheduled and carried out with the FOC using three different filter sets. They were: 1) Caldwell et al. (F140W & F152M), 2) Paresce et al. (F120M &F140W), and 3) Stern et al. (F130M & F140W). The observations were obtained from February 6-9, 1992 in the four days surrounding the Ulysses spacecraft's closet approach to Jupiter. The images reported here are from the Stern, McGrath, Waite, Gladstone, and Trafton investigation using the FOC in a f/96 512 by 512 pixel mode (F96N512) with filters F130M and F140W that have a peak spectral response near 1280 angstroms. The field-of-view was 11 x 11 arcseconds and the exposure time for each of the eight images was 18 minutes. The center of the field-of-view was offset 20 arcseconds toward the appropriate Jupiter rotational pole during each observation with a pointing accuracy of approximately 1 arcsecond. For a point of reference Jupiter's polar radius during the time of these observations was approximately 20.54 arcseconds. A summary of the images obtained is shown in Table 1 where we have listed the time of observation, the S_{III} longitude of the central meridian at the midpoint of the observation, the pole observed, the intensity of noticeable features in the image, the emission area, and a rough estimate of the range of the emission power (taking into account the low signal to noise ratio of the data, the difficulty in determining the physical area of the emission, and the uncertainties due to atmospheric absorption).

The determination of the auroral emission power requires that a convolution of the FOC wavelength dependent quantum efficiency (QE) and filter response functions be convoluted with

the auroral H, H_2 spectrum. This was accomplished by modeling both the altitude dependent Lyman alpha and H_2 Lyman and Werner production rate profiles [Waite et al., 1983] assuming a low latitude hydrocarbon vertical distribution [Gladstone and Skinner, 1989] and a precipitating electron spectrum consistent with those observed by Ulysses in the outer magnetosphere [Lanzerotti et al., 1992] and extended down to energies of 20 KeV (below the detector threshold of 44.9 KeV) with the same power law slope in the distribution. The extension to lower electron energies was performed to match the H_2 band color ratio (a measure of the lower energy extent of the precipitating electron distribution for a specified methane vertical profile) generally observed in the Jovian auroral zone [Yung et al., 1980; Waite et al., 1988]. These production rate values were then used as input to a radiative transfer code [Gladstone and Skinner, 1988] (for output see Figure 1a) and then passed through an FOC QE/filter response to produce the synthetic spectrum seen in Figure 1b. As you can see the F130M F140W filter pair responds to both Lyman alpha and Werner band emission near 1280 angstroms, whereas the Paresce images are more sensitive to Lyman alpha and the Caldwell images to Lyman emission near 1580 angstroms. The latter wavelength region is less susceptible to methane absorption, thus it's specification in the upper wavelength range of the Yung et al. [1980] H_2 band color ratio:

CR= Intensity(1557-1619 angstroms)/Intensity(1230-1300 ang.)

A comparison of the relative spectral responses of the three different filter combinations is shown in Table 2. In order to verify that this approach for determining the integrated auroral flux from the limited bandpass 130M 140W combination was not overly sensitive to the assumed methane vertical profile or to the assumed electron energy spectrum used in the modeling we repeated the QE/filter convolution with a measured IUE Jovian auroral spectrum and got the same result to within 20%. We then used the predicted FOC count rates and compared them to the measured rates along with constants that define the telescope's effective area to estimate the power influx levels required to produce the observed auroral emissions (shown in Table 1).

Two images of the north auroral zone (NAZ) and six images of the south auroral zone (SAZ) were obtained over the 4 day span. Five images (1 of the NAZ, 4 of the SAZ) showed emission (>1 sigma) above the image dark count. These five images are shown in Figures 2a and 2b. The image has been processed using a 10 pixel box car average and the color bar has been dynamically stretched to provide a common intensity representation from image to image while at the same time maximizing contrast in the low signal to noise level images. The average background count rate in the five processed images was 0.598 +/- 0.088 counts per pixel, whereas the count rate on the planet without auroral emission was 0.0654 +/- 0.094 counts per pixel. This suggest, as the images indicate, that there is no statistically visible planet limb to aid in interpreting the planetary coordinates. The limb and auroral zone overlays that are shown are determined by constructing a planetary coordinate grid and two sets of auroral zones: 1) L=6, associated with the Io plasma torus, and 2) L=infinity, associated with the last closed magnetospheric field line using the O_4 magnetic field model [Acuna and Ness, 1976] and an IDL program written by Dr. Tim Livengood to process IUE spectra from Jupiter. The finite spread to the auroral zones shown are simply due to the rotation of the planet during the 18 minute exposure. Peak count rates on the images lie between 0.88 and 1.67 counts per pixel which

corresponds to auroral intensities between 20 and 50 kiloRayleighs (kR), yet the low sensitivity of the dual filter FOC combination sets a detection threshold range between 10 and 20 kR. As such only the brighter auroral features are visible in the images and low emission intensities over large areas can mask large uncertainties in the auroral power (See Table 1; image features 101b, 101c, 302b, and 402b where an attempt has been made to estimate the emission uncertainty associated with diffuse emissions over large areas. The selected regions are shown in Figure 3 where a 10 by 10 block average representation of the image with a box overlay designating the selected areas are shown and Table 3 where the average count values and their associated uncertainties are listed.)

The NAZ image (image #101 in Table 1) shows a bright central feature near the Central Meridian Longitude (CML= 163-173 degrees S_{III} longitude) and therefore a reasonable estimate of the S_{III} longitude of the emission feature can be estimated and lies between 160 and 173 degrees. The bifurcated nature of the source can be explained by either spatial (5 degrees of longitude) or temporal (10 minutes, due to planetary rotation during the exposure) variability in the source. The bright source location (image #101a) is most consistent with a middle magnetospheric source (halfway between L=6 and the last closed magnetospheric field line), but a pointing uncertainty of about 1 arcsecond (the size of the marker for celestial N and E) spans the range of auroral zones considered and makes the designation tentative at best. Some weaker emission (image #101b) poleward and westward of the central bright spot is just barely visible above the background as is the area (#101c) to the east of the bright central spot. These areas may represent a weaker "polar oval" emission that is more clearly seen at longer wavelengths in the images of Caldwell et al. (EOS,??). The other NAZ image (#102) suffers from a high noise level that negates meaningful analysis.

The first SAZ image is (image #201 from Table 1). In this image most of the emission appears to lie along the limb of the planet, thus making it difficult to estimate the longitudinal position and intensity of the emission. The CML of this image is 43 degrees S_{III}. Most of the emission appears to lie near a longitude of 180 degrees (#201a, westward edge of auroral zone), but another weaker (?) zone appears near 0 degrees (#201b, eastward edge of the auroral zone). However, image #202 taken 1 hr 27 mn later at a CML longitude of 95 degrees shows emission from the center of the imaged auroral zone (near 100 degrees) and suggests that significant changes in the auroral zone morphology occurred in the intervening time period. The extent of the limb emissions are most consistent with an auroral zone size which corresponds to the boundary of the last closed field lines (ie., maps to near the magnetopause boundary). The intensities listed in Table 1 for this image are uncertain due to the presence of limb brightening effects.

The image pair 301 302 provide information about the temporal variability of the auroral emissions. Image #301 (CML=5 degrees) shows no detectable emission above the background. Whereas, image #302 (CML=56 degrees) shows a bright emission feature between 20 and 30 degrees; a region that should have been clearly visible if present 1 hr 28 mn earlier in image #301. This suggest over a factor of three variation in the auroral intensity during the time period spanned by these two images. Image #302 is also particularly interesting from a Ulysses

encounter point of view, since at the time of the image the HISCALE experiment [Lanzerotti et al., 1992] had just been turned on after closet approach and was observing precipitating energy fluxes of electrons on the order of 1 erg cm^{-2} s^{-1} (~20 kR of emission corresponding to light blue areas just above the background) at the dusk edge of the planet (S_{III}~305 degrees, L~16). Although the conjugate auroral point is just off the field of view of the image a duskward extension of the diffuse auroral emission seen surrounding the central bright spot in an auroral band at L>16 is of a consistent brightest and location to correspond to the measured electrons of HISCALE. Again as in image 201 the auroral zone is more consistent with a mapping to L>15, yet here again pointing uncertainties must be carefully considered. Once again as in image #101 the complex structure of the central bright emission features can be explained by a combination of temporal and spatial structure of the auroral precipitation zones. As a matter of fact in image #302 some of the structure must be spatial because the large separation (>1 arcseconds) of hot spots cannot be explained by rotation of a time variable source alone.

Finally the image pair 401 402 again illustrate both the temporal and spatial variability of the source. No detectable emission above background is seen in image #401 (CML=350-360 degrees), but 1 hr 26 mn later an emission (image #402a) appears near 300 degrees CML; a longitude range that should have been visible in image #401. The magnetic latitude in 402 is again more consistent with auroral emission that maps to the magnetopause boundary than with emission that maps to the Io plasma torus.

HST FOC Images: Discussion

A major consideration in placing these HST FOC images in the context of past Voyager UltraViolet Spectrometer (UVS) and International Ultraviolet Explorer (IUE) observations is the low signal to noise ratio of the images and the resulting sensitivity threshold between 10 and 20 kR of emission over large areas of the high latitude region which would not be visible above the background. Clearly these images are a high spatial resolution tracer of the variations in the auroral bright spots and not as good of an indicator of the more diffuse auroral emission or correspondingly of the total auroral power output. Integrated power numbers for the input power required to produce these bright emissions range from 10^{10} to 10^{12} Watts in both the SAZ and NAZ. However, if we assume that a 20 kR band from 65 to 85 degrees may exist below the detection limit of the FOC then up to 4 x 10^{13} W of input power may be present, but unaccounted for by the present observations. This also would imply that less than 10% of the emission is found in the bright spots, whereas Herbert et al.'s [1987] analysis of the Voyager data suggest that between 20 and 30% of the emission is concentrated in the bright auroral emission regions. Furthermore, Herbert et al. [1987] give estimates of the emitted power (in their Table 2) which can be used to estimate the input power using the emissions efficiencies given by Waite et al. [1983]. Their results give values for the total auroral power input for Voyager 1 inbound of 1.2 x 10^{14} Watts and for the outbound 4 x 10^{13} Watts and an estimate for Voyager 2 of 1.1 x 10^{14} Watts. Livengood [1991] has performed an extensive analysis of the IUE Jovian aurora data set. Using the information from Figure 5.9 of Livengood [1991] and the modeled emission efficiencies from Waite et al. [1983] we obtain an average auroral H, H_2 emission power of 4.4 x 10^{12} Watts (both poles) and an input power of 2.4 x 10^{13} W with a one sigma variance of ~1

x 10^{13} Watts and individual data points that show up to a factor of six variation in the emitted power over the span of less than one month. The limited data set of Livengood [1991] spans over 10 years with relatively greater sampling since 1988, but there are no indications of a long term trend in the auroral power output. Placing the measured and inferred auroral power output of the FOC images in the context of the UVS and IUE data suggest that: 1) the majority of the emitted auroral power is in diffuse and weak features below the sensitivity threshold of the FOC, 2) the auroral output power during the Ulysses encounter was in the range of it's observed average as determined by IUE (1 to 3 x 10^{13} Watts), and 3) the aurora is randomly time variable on time scales as short as 10 minutes (given a temporal interpretation of the bifurcation of the bright spot in image #101), and certainly varies by over a factor of three in brightness on time scales of hours.

The UVS and IUE data sets also indicate a systematic variation of the intensity of the auroral emissions in both the NAZ and SAZ as a function of S_{III} longitude. Although these bright regions are identified in the FOC data set (image #101 for the NAZ, central bright spot at ~170 degrees; image #302 for the SAZ, central bright spot at ~25 degrees), the considerable spatial and temporal variation that occurs in time spans of less than two hours in the set of eight FOC images reported here suggest a much more complex pattern of variability (at least for the brightest auroral emissions) and further suggest that part of the systematic variance from IUE and UVS may be due to geometrical considerations of a large spectrometer slit viewing an increasing area of diffuse and distributed auroral emission at certain preferred S_{III} longitudes.

Information on the spectral variations of the Lyman alpha and Lyman and Werner band systems cannot be inferred from the single filter set used in the reported FOC images. As a result, information about the H_2 band color ratio as a function of longitude reported by both IUE and UVS, which gives information on the input particle energy spectrum and/or the changes in the hydrocarbon atmosphere, cannot be compared at present. However, by mixing the different images from the three sets of observations it may be possible to draw some conclusions about systematic variations in the emission spectrum (see Table 3). The one caveat is the high degree of variability will make any spectral comparison from one image to the next hard to quantify.

The most exciting new piece of information comes from the high spatial resolution that can be obtained from HST. The small bright discrete sources seen in the data set put obvious constraints on the magnetospheric processes responsible for the precipitating particles. This patchy and discrete structure is also present in the observed high-latitude magnetospheric particle populations observed by the HISCALE particle detector on the Ulysses spacecraft [Lanzerotti et al., 1992]. Furthermore, the location of the discrete features in latitude (although individually accurate to one arcsecond due to pointing uncertainties) collectively are consistent with a precipitating particle origin in the middle (NAZ) or outer (SAZ) magnetosphere, which is again consistent with the measurement by HISCALE of precipitating electrons in the middle and outer magnetosphere. The limited data available, however, make a comparison to Voyager UVS derived auroral zone [Herbert et al., 1987] difficult to carry and further HST observations are needed to verify the present result. The inference to be drawn from this information is that the Jovian aurora is more Earth-like than previously thought and that acceleration of electrons carrying field-aligned currents in the middle and outer magnetosphere may be largely responsible for the

discrete auroral emission features seen by HST in the southern auroral zone.

ROSAT Observations

The ROSAT Position Sensitive Proportional Counter (PSPC) acquired nine data segments between April 23, 1991 and April 25, 1991 that have the Jupiter disk within the field of view. The times for each segment are listed below in Table 4. Due to the low count rates in each of the individual data segments the portion of the image which contained the disk of Jupiter (with a factor of two spatial margin) was extracted from each of the nine data segments, individual background subtractions using clear sky were performed, and the resulting data was combined into a single spectra. Therefore no information exist about the possible variation of the spectra as a function of Jupiter rotational phase. However, the single spectrum has been thoroughly analyzed in the context of a best fit bremsstrahlung and a best fit two emission line model. The data along with the results of these best fit models are shown in Figure 4. Please note that the model fits have been convolved with the proper energy resolution and energy dependent quantum efficiencies to allow a comparison with the extracted PSPC data. Therefore, the data shown are not to be interpreted as spectra, but as spectra convoluted with the PSPC response function. Although, the signal to noise is low in the data set due to the small amount of on-Jupiter observation time in the present data set, the two line model is clearly a better fit with a chi square that is over a factor of two better than the best fit bremsstrahlung model (and also a factor of two better than the best power law fit which is not shown in the figure).

ROSAT Discussion

The total x ray power inferred from the analysis is 1.3 to 2.1 x 10^9 Watts depending on whether the model fit assumed is the two line or the bremsstrahlung, respectively. This is within a factor of three of the 4 x 10^9 Watts reported from the Metzger et al. [1983] Einstein x ray observations. The observed comparison is within variations that are associated with changes in the ultraviolet auroral output [Livengood, 1991]. Furthermore, in agreement with Metzger et al. we conclude that from bremsstrahlung x ray modeling that the model efficiency (5.6 x 10^{-7}; Waite, 1991) suggests that over 3 x 10^{15} Watts of auroral electron precipitation would be required to produce the observed x ray emission from an electron bremsstrahlung source. However, the factor of two better energy resolution available with ROSAT (as compared to Einstein) also allows a spectral interpretation of the results. This data as shown in Figure 4 suggests that a two line emission model produces a better fit (by a factor of two in chi square) than does the best bremsstrahlung fit. Yet the line model fit has two components, a narrow component near 0.2 KeV and a broader component centered at 0.9 KeV, which are not consistent with the Metzger et al. interpretation of S and O K-shell emission at 2.3 and 0.52 KeV, respectively. Reference to the soft x ray emission tables of Raymond and Smith [1977] does indicate a series of S(VII) recombination lines near 0.2 KeV and a series of O(VII) recombination lines near 0.9 KeV which are strong candidates for explaining the observed emissions (see Figure 5). The production of these emission lines occurs as a result of recombination lines that are produced from the slowing of the energetic ion beam as it enters the Jupiter upper atmosphere.

Charge state equilibrium of the ion beam in the atmosphere results from competition between electron capture and stripping which are charge state and energy dependent.

Stripping: $S, O^{+(q-1)} + H, H_2 \rightarrow S, O^{+q} + H, H_2 + e^-$

Capture: $S, O^{+q} + H, H_2 \rightarrow S, O^{+(q-1)} + H, H_2^+$

We estimate that in the electron capture process 10% of the reaction exothermicity goes into the excitation of recombination lines. If the initial charge states are S(VII) and O(VII) the resulting emission is in the soft x ray wavelength regime.

Recombination excitation:

$$S(VIII), O(VIII) + H, H_2 \rightarrow S(VII), O(VII)^* + H, H_2^+$$

$$S(VII), O(VII)^* \rightarrow S(VII), O(VII) + \text{x ray}$$

The high charge states necessary to produce these emissions are the result of the incident ion beam energy and the fact that electron stripping and capture processes result in a rapid charge state equilibrium being established as the beam encounters the upper atmosphere. This point is illustrated (Figure 6) for energetic oxygen where we have presented the equilibrium fraction of the various charge states as a function of beam energy (results from private communication with T. E. Cravens, 1992). The figure indicates that an O(VII) charge state will occur for all ions that enter the atmosphere with an energy greater than ~700 KeV per amu. That such ions exist in the Jupiter magnetosphere and probably precipitate between L=7 and 10 has been demonstrated using Voyager data by Gehrels and Stone [1983]. They estimate that between 10^{12} and 10^{13} Watts of oxygen and sulfur with energies greater than 700 KeV per amu is precipitating into the Jupiter. This implies that an efficiency of 0.01 to 0.1% is required from x ray recombination processes to explain the present x ray aurora in a manner consistent with the observed loss of energetic oxygen and sulfur by Voyager [Gehrels and Stone, 1983]. Such an efficiency appears to be quite reasonable in the context of the modeling of energetic oxygen aurora at Jupiter by Horanyi et al. [1988] and detailed modeling calculations are now in progress.

However, we further note that as pointed out by Gehrels and Stone [1983] the observed energetic ion precipitation does not contain sufficient power to explain the observed ultraviolet aurora and extrapolations to 40 KeV per amu are required to supply this additional power. Such an extrapolation is not necessary to explain the observed x ray emissions. We therefore, conclude that in light of the HST Ulysses results, both electrons and ions play a role in the Jupiter auroral emissions, but that the bulk of the ultraviolet emissions (and thus a major portion of the power input) comes from electron processes, which result from processes in the outer magnetosphere and not from energetic ions precipitating from the middle magnetosphere. Such a scenario forms the new paradigm of the Earth-like aurora at Jupiter.

References

Acuña, M. H., and N. F. Ness, Results from the GSFC fluxgate magnetometer on Pioneer 11, in *Jupiter*, edited by T. Gehrels, p. 830-847, University of Arizona Press, Tucson, 1976.

Broadfoot, A. L., et al., Overview of the Voyager ultraviolet spectrometry results through Jupiter encounter, *J. Geophys. Res., 86*, 8259-8284, 1981.

Caldwell, J., A. T. Tokunga, and G. S. Orton, Further observations of 8 μm polar brightenings of Jupiter, *Icarus, 53*, 133-140, 1983.

Caldwell, J., A. T. Tokunga, and F. C. Gillett, Possible infrared aurorae on Jupiter, *Icarus, 44*, 667-675, 1980.

Caldwell, J., *EOS*???

Clarke, J. T., H. W. Moos, S. K. Atreya, and A. L. Lane, Observations from Earth orbit and variability of the polar aurora on Jupiter, *Astrophys. J. (Lett.)., 241*, L179-182, 1980.

Dols, V., J. C. Gerard, F. Paresce, R. Prange, and A. Vidal-Madjar, Ultraviolet imaging of the Jovian aurora with the Hubble Space Telescope, in press *GRL*, 1992.

Gehrels, N., and E. C. Stone, Energetic oxygen and sulfur ions in the Jovian magnetosphere and their contribution to the auroral excitation, *J. Geophys. Res., 88*, 5537-5550, 1983.

Gladsstone, G. R., and T. E. Skinner, Spectral analysis of Jovian auroral emissions, in *Time-Variable Phenomena in the Jovian System*, M. J. S. Belton, R. A. West, and J. Rahe, Eds., NASA SP-494, Washington, D. C., 221-228, 1989.

Herbert, F., B. R. Sandel, and A. L. Broadfoot, Observations of the Jovian UV aurora by Voyager, *J. Geophys. Res., 92*, 3141-3154, 1987.

Horanyi, M., T. E. Cravens, and J. H. Waite, Jr., The precipitation of energetic heavy ions into the upper atmosphere of Jupiter, *J. Geophys. Res., 93*, 7251-7271, 1988.

Lanzerotti, L. J., T. P. Armstrong, R. E. Gold, K. A. Anderson, S. M. Krimigis, R. P. Lin, M. Pick, E. C. Roelof, E. T. Sarris, G. M. Simnett, C. G. Maclennan, H. T. Choo, and S. J. Tappin, Hot plasma environment at Jupiter: Ulysses results, in press *Science*, 1992.

Livengood, T. A., R. M. Prangé, G. E. Ballester, and H. W. Moos, Exceptional variability of the Jovian ultraviolet aurora of December 1990: Primary particle energy and identity?, *EOS Trans. AGU, 72*, 185, 1991.

Metzger, A. E., D. A. Gilman, J. L. Luthey, K. C. Hurley, H. W. Schnopper, F. D. Seward, and J. D. Sullivan, The detection of X-Rays from Jupiter, *J. Geophys. Res., 88*, 7731-7741, 1983.

Raymond, J. C., and B. W. Smith, Soft x ray spectra of a hot plasma, *App. J. Suppl., 35*, 419-439, 1977.

Sandel, B. R., et al., Extreme ultraviolet observation from Voyager 2 encounter with Jupiter, *Science, 206*, 962-966, 1979.

Waite, J. H., Jr., Comment on "Bremsstrahlung X rays from Jovian auroral electrons" by D. D. Barbosa, *J. Geophys. Res., 96*, 19,529-19,532, 1991.

Waite, J. H., Jr., J. T. Clarke, T. E. Cravens, and C. M. Hammond, The Jovian aurora: Electron or ion precipitation?, *J. Geophys. Res., 93*, 7244-7250, 1988.

Waite, J. H., Jr., et al., Electron precipitation and related aeronomy of the Jovian thermosphere and ionosphere, *J. Geophys. Res., 88*, 6143-6163, 1983.

Yung, Y. L., et al., H_2 fluorescence spectrum from 1200 to 1700Å by electron impact: Laboratory study and application to Jovian aurora, *Astrophys. J. (Lett.)., 254*, L65, 1982.

Yung, Y. L., and D. F. Strobel, Hydrocarbon photochemistry and Lyman alpha albedo of Jupiter, *Astrophys. J., 238*, 395-402, 1980.

Figure Captions

Figure 1a. Model Jovian auroral spectrum of the H Lyman alpha and H_2 band emissions.

Figure 1b. The convolution of the model spectrum with the wavelength dependent filter and quantum efficiencies response curves for the HST FOC F130M/F140W.

Figure 3. Ten by ten block averaged representation of the full set of HST FOC images with boxes indicating positions of intensity information extraction.

Figure 4. Combined ROSAT PSPC photon energy spectrum and the model curves for a best fit two line model and a best fit bremsstrahlung model convoluted with the detector response function.

Figure 5. Two line model fit and the wavelength location and relative intensity of known recombination emission lines from S(VII) and O(VII).

Figure 6. Equilibrium fraction for O^{+q} (q = 0, 8) charge state distributions as a function of ion energy.

Table 1. HST Jovian Auroral Observations

I#	DATE	TIME(UT)	CML(S_{III})	POLE	Intensity(kR)	Area($''^2$)	Power(W)*
101a	2/6/92	2:40	168	North	34 +/- 23	2.9	$5x10^{10}$ - $7x10^{11}$
101b	2/6/92	2:40	168	North	13 +/- 14	2.8	0 - $5x10^{12}$
101c	2/6/92	2:40	168	North	31 +/- 34	1.1	0 - $2x10^{13}$
102	2/6/92	4:08	222	North	High Noise	---	---
201a	2/7/92	9:07	43	South	12 +/- 11	4.8	$1x10^{10}$ - $5x10^{11}$
201b	2/7/92	9:07	43	South	24 +/- 18	2.5	$2x10^{10}$ - $5x10^{11}$
202	2/7/92	10:34	95	South	49 +/- 30	1.7	$1x10^{11}$ - $5x10^{11}$
301	2/8/92	23:46	5	South	Low Signal	---	---
302a	2/9/92	1:11	56	South	26 +/- 21	2.6	$1x10^{10}$ - $5x10^{11}$
302b	2/9/92	1:11	56	South	8 +/- 16	2.1	0 - $4x10^{12}$
401	2/9/92	9:24	355	South	Low Signal	---	---
402a	2/9/92	10:50	47	South	41 +/- 28	1.8	$2x10^{10}$ - $1x10^{12}$
402b	2/9/92	10:50	47	South	22 +/- 24	1.6	0 - $1x10^{13}$

* Range limits include not only 1 sigma measurement uncertainties, but also a factor of 2 uncertainty due to unaccounted for atmospheric absorption, a factor of 2-4 increase from the optical defects of HST which depends on the size of the emission region, and an upper limit to the size of the emitting area

Table 2. Spectra for Caldwell, Stern, and Paresce

BAND	CALDWELL (F140W, F152M)	STERN (F130M, F140W)	PARESCE (F120M, F140W)
Lya	0.034	0.340	0.828
1230-1650	0.962	0.648	0.149
1230-1300	0.015	0.385	0.106
1557-1619	0.290	0.010	0.004
Total (cps/pixel)	1.64E-5	6.21E-6	1.29E-5

Table 3. HST FOC Intensity Determination

DESIGNATED IMAGE BLOCK		IMAGE COORDINATES [X1:X2, Y1:Y2]	AVERAGE COUNTS AND VARIANCE (per pixel)
Image 101	101a	[16:23, 14:23]	0.95±0.21
	101b	[10:16, 28:38]	0.74±0.11
	101c	[31:35, 4:10]	0.73±0.10
	bc1(101)	[5:13, 3:13]	0.63±0.09
	[off planet]		
	bc2(101)	[34:44, 34:44]	0.61±0.09
	[on planet, no aurora]		
Image 102	no analysis attempted due to high noise level		
Image 201	201a	[10:18, 25:38]	0.90±0.16
	201b	[36:42, 2:11]	0.91±0.12
	bc1(201)	[4:14, 4:14]	0.62±0.08
	bc2(201)	[25:35, 25:35]	0.70±0.10
Image 202	202	[20:26, 22:28]	0.88±0.14
	bc1(202)	[5:15, 5:15]	0.56±0.09
	bc2(202)	[30:40, 30:40]	0.60±0.09
Image 301	no analysis attempted due to low signal level		
Image 302	302a	[29:37, 7:14]	1.00±0.16
	302b	[24:29, 20:29]	0.83±0.12
	bc1(302)	[5:15, 5:15]	0.66±0.09
	bc2(302)	[30:40, 30:40]	0.77±0.11
Image 401	no analysis attempted due to low signal level		
Image 402	402a	[29:37, 4:9]	0.85±0.12
	402b	[24:29, 17:24]	0.71±0.10
	bc1(402)	[5:15, 5:15]	0.52±0.09
	bc2(402)	[30:40, 30:40]	0.59±0.08

Table 4. Segment Times

START (UT)		STOP
4/23/91	12:52:32	13:01:55
4/23/91	22:03:42	22:31:58
4/24/91	03:11:37	03:26:58
4/24/91	12:51:27	13:00:54
4/24/91	19:00:44	19:12:41
5/24/91	03:10:28	03:24:53
5/24/91	11:15:52	11:23:17
5/24/91	12:42:06	12:59:11
5/24/91	17:22:04	17:40:20

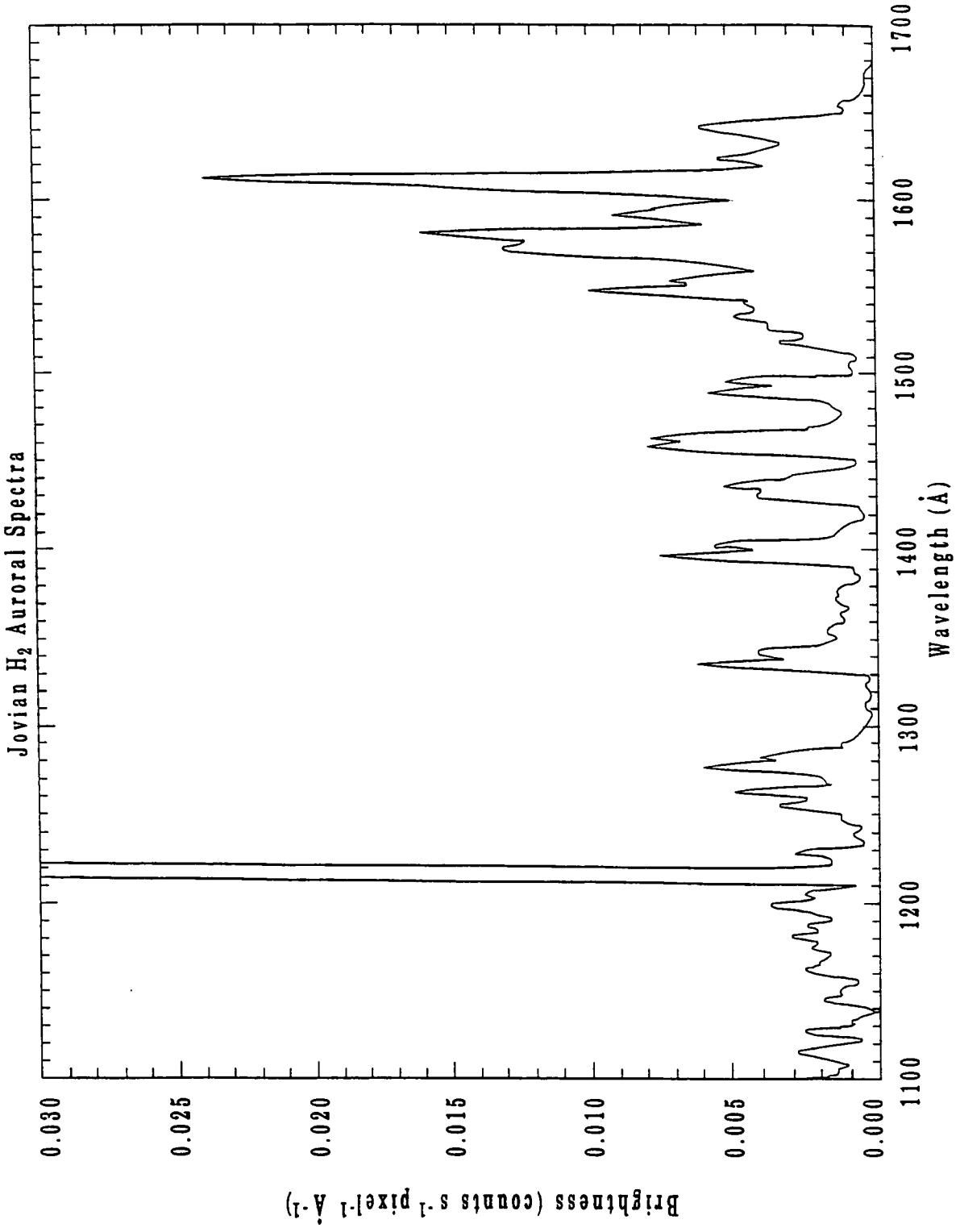
Jovian H_2 Auroral Spectra
Brightness (counts s^{-1} $pixel^{-1}$ $Å^{-1}$)
Wavelength (Å)
0.030
0.025
0.020
0.015
0.010
0.005
0.000
1100
1200
1300
1400
1500
1600
1700

Figure 1a

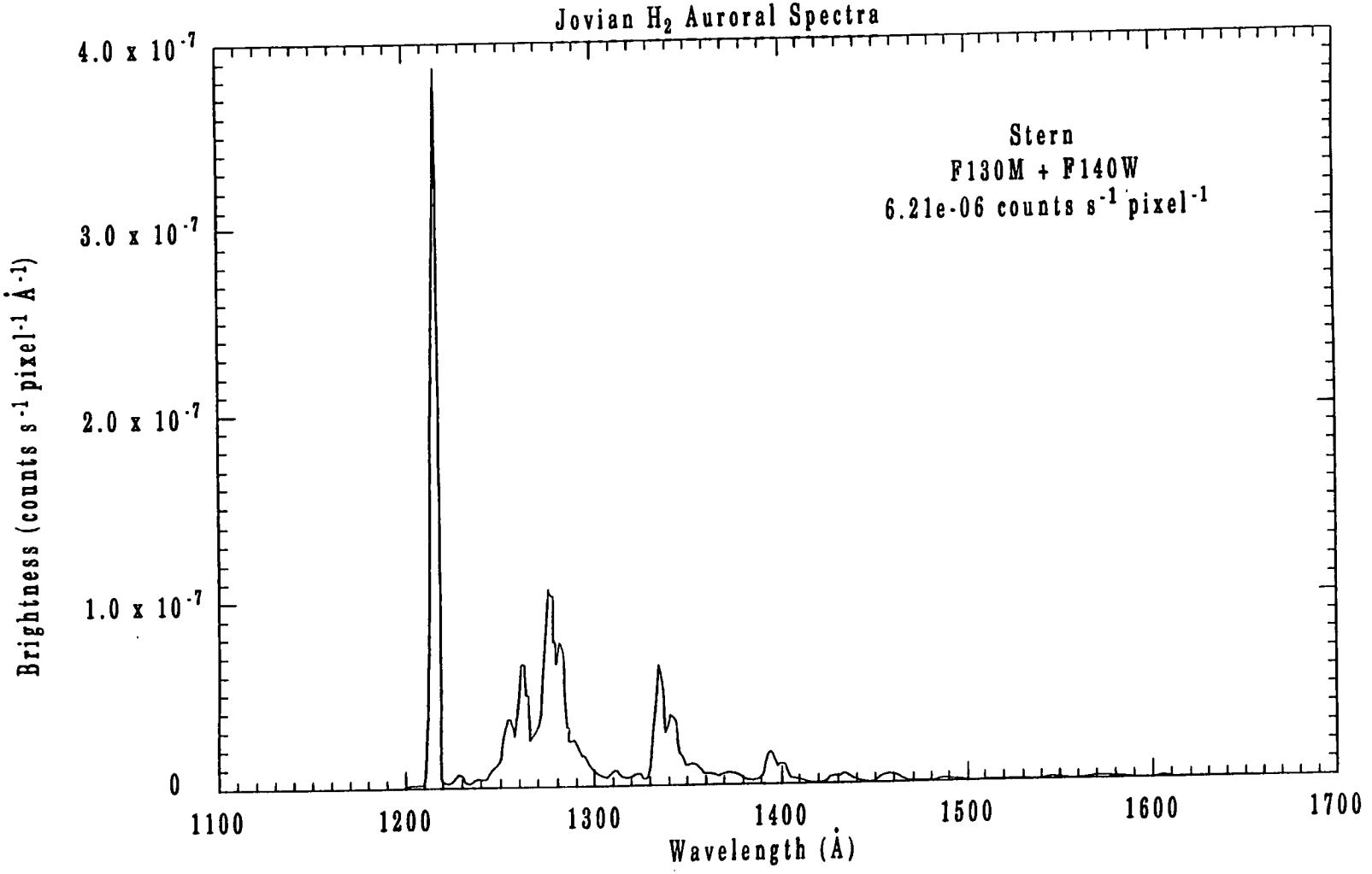
Jovian H_2 Auroral Spectra
Stern
F130M + F140W
6.21e-06 counts s^{-1} $pixel^{-1}$
Brightness (counts s^{-1} $pixel^{-1}$ Å^{-1})
4.0 x 10^{-7}
3.0 x 10^{-7}
2.0 x 10^{-7}
1.0 x 10^{-7}
0
1100
1200
1300
1400
1500
1600
1700
Wavelength (Å)

Figure 1b

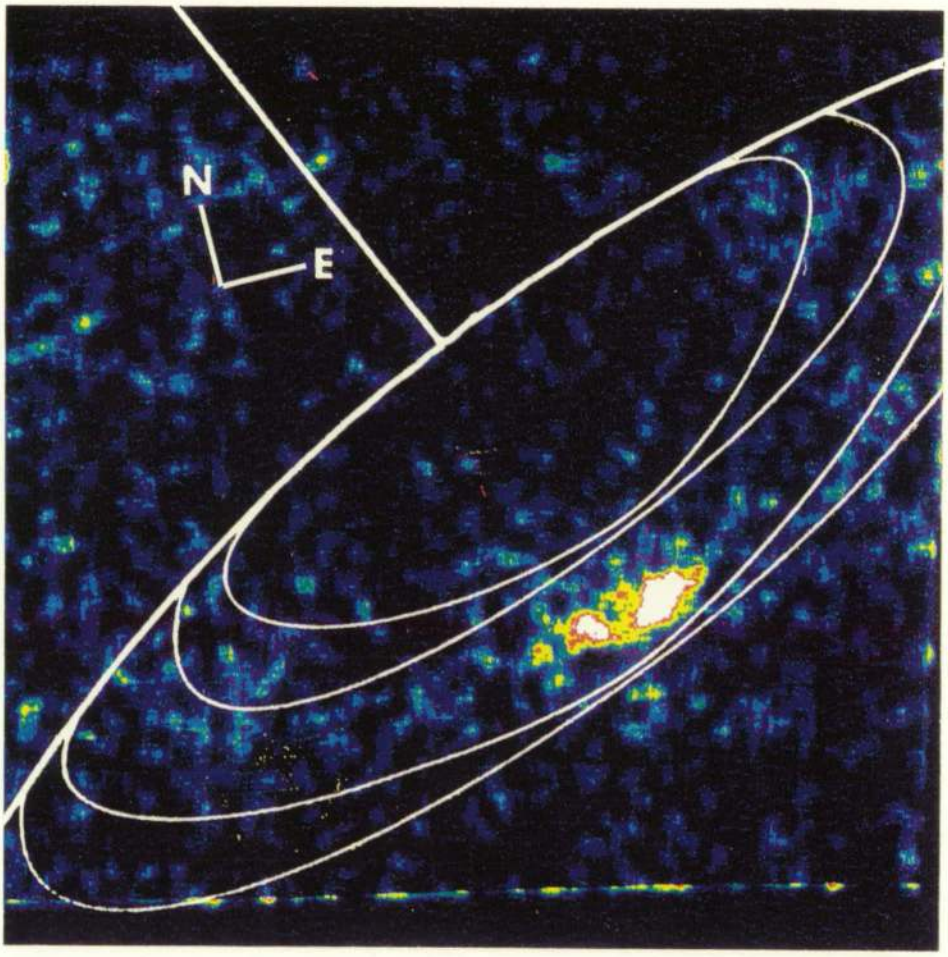

Figure 2a. Reduced HST FOC image of the north pole showing bright auroral features and shading that indicate Jovian magnetic coordinates for Io plasma torus auroral zone low latitude circle and magnetopause auroral zone smaller inner circle.

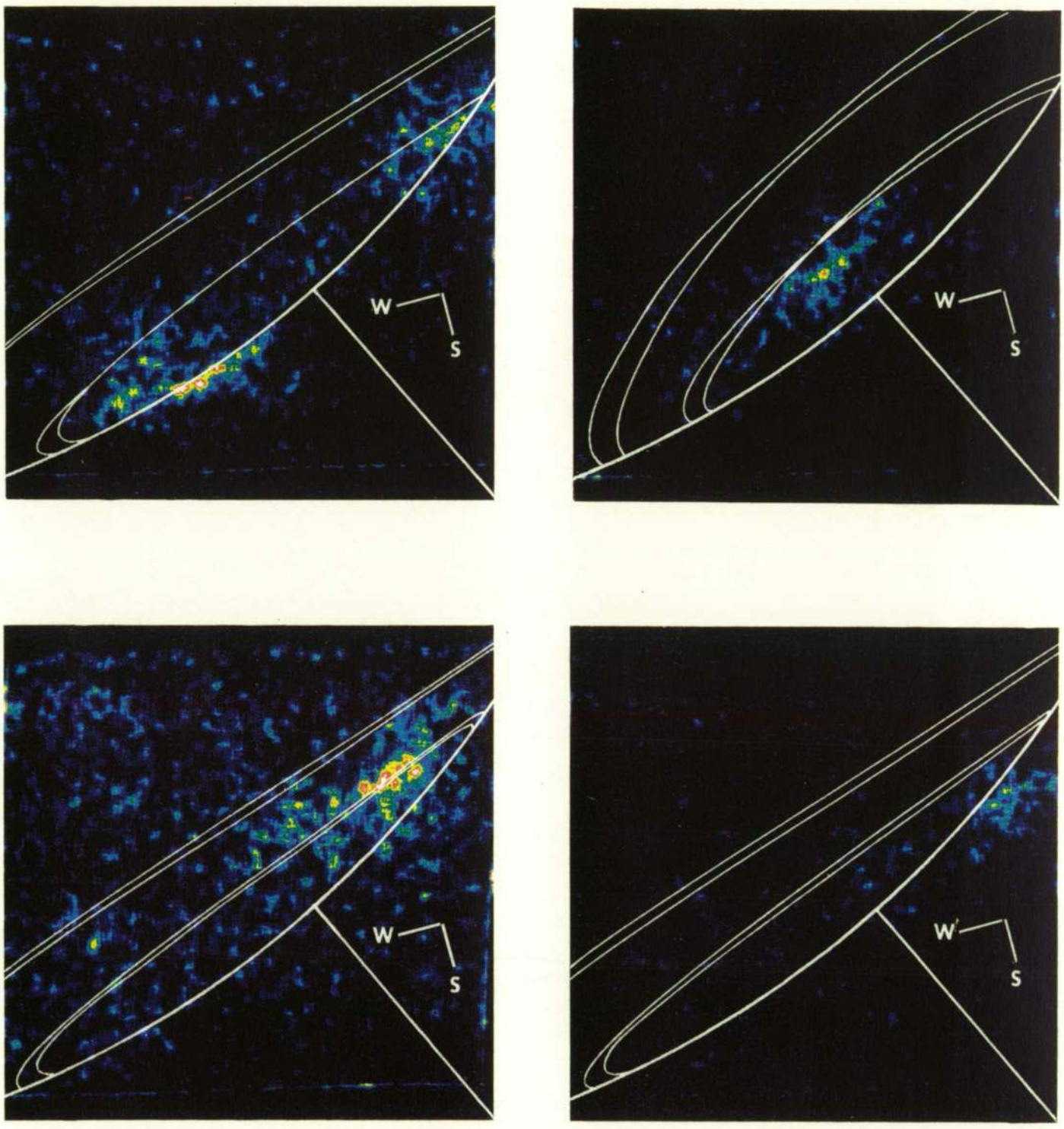

Figure 2b. Reduced HST FOC images of the south pole showing bright auroral features and shading that indicate Jovian magnetic coordinates for Io plasma torus auroral zone low latitude circle and magnetopause auroral zone smaller inner circle.

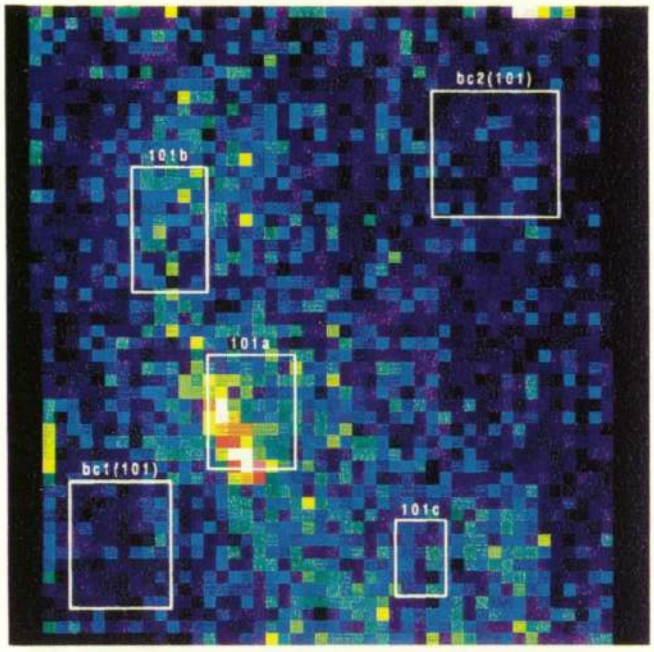

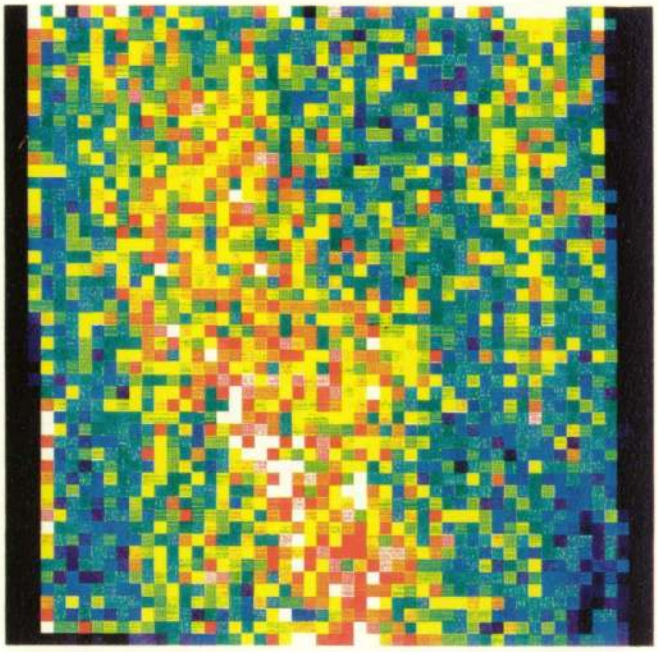

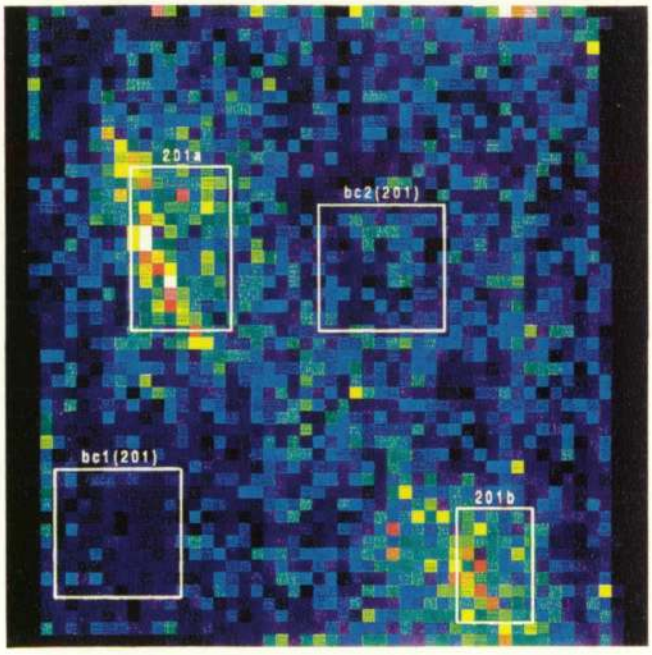

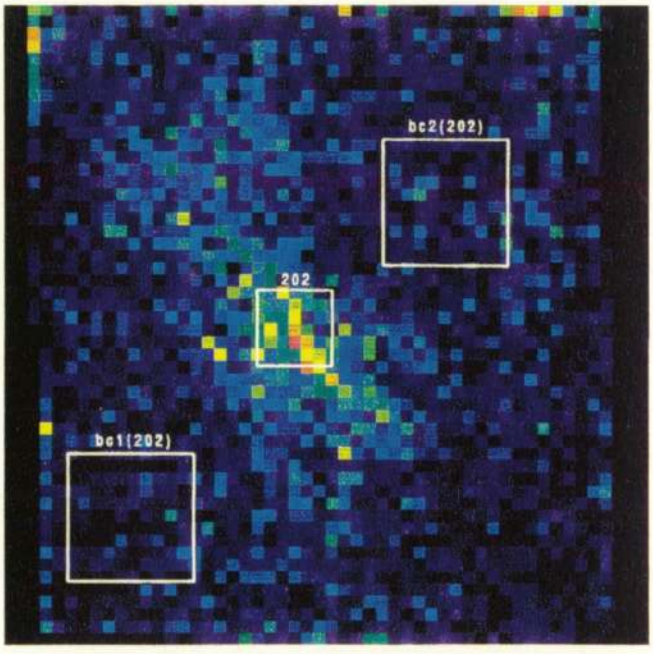

Figure 3a

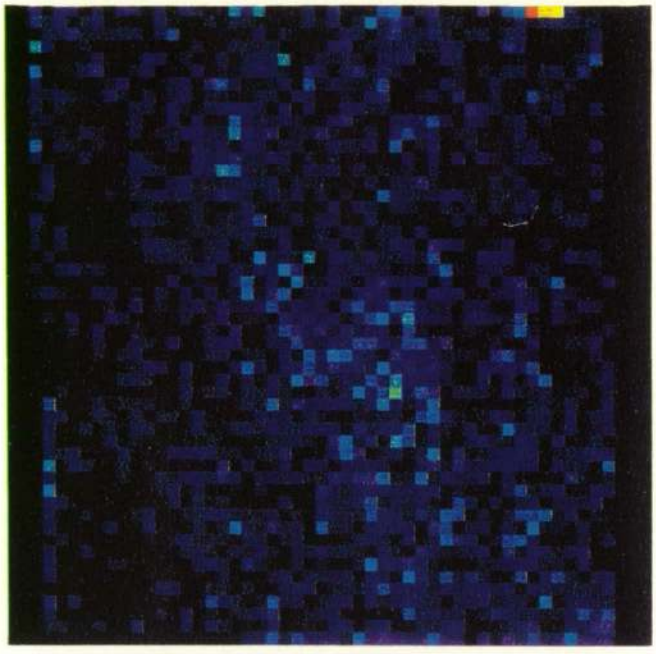

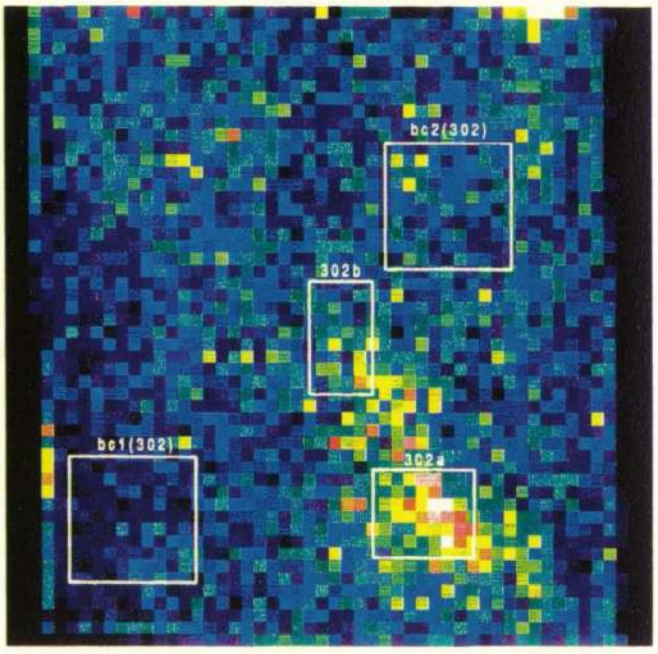

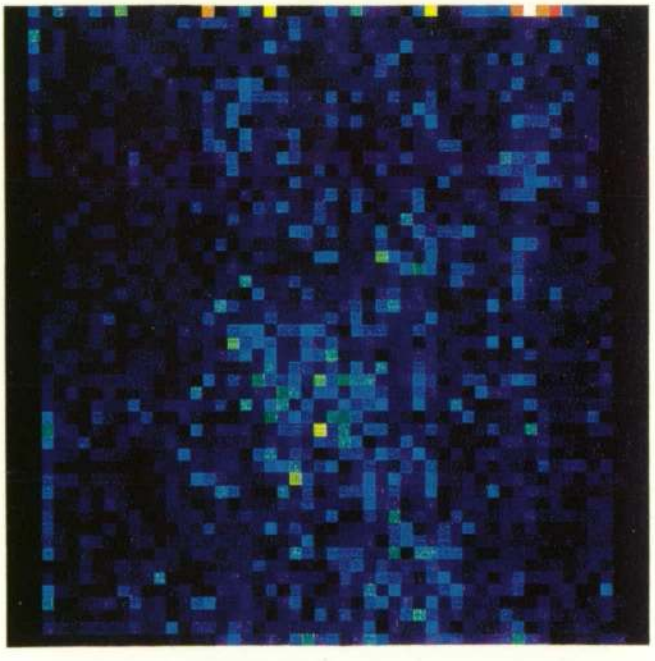

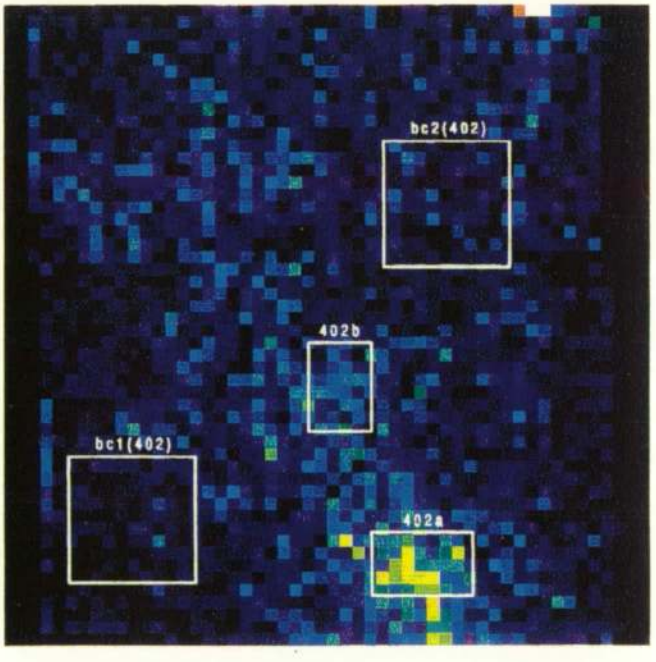

Figure 3b

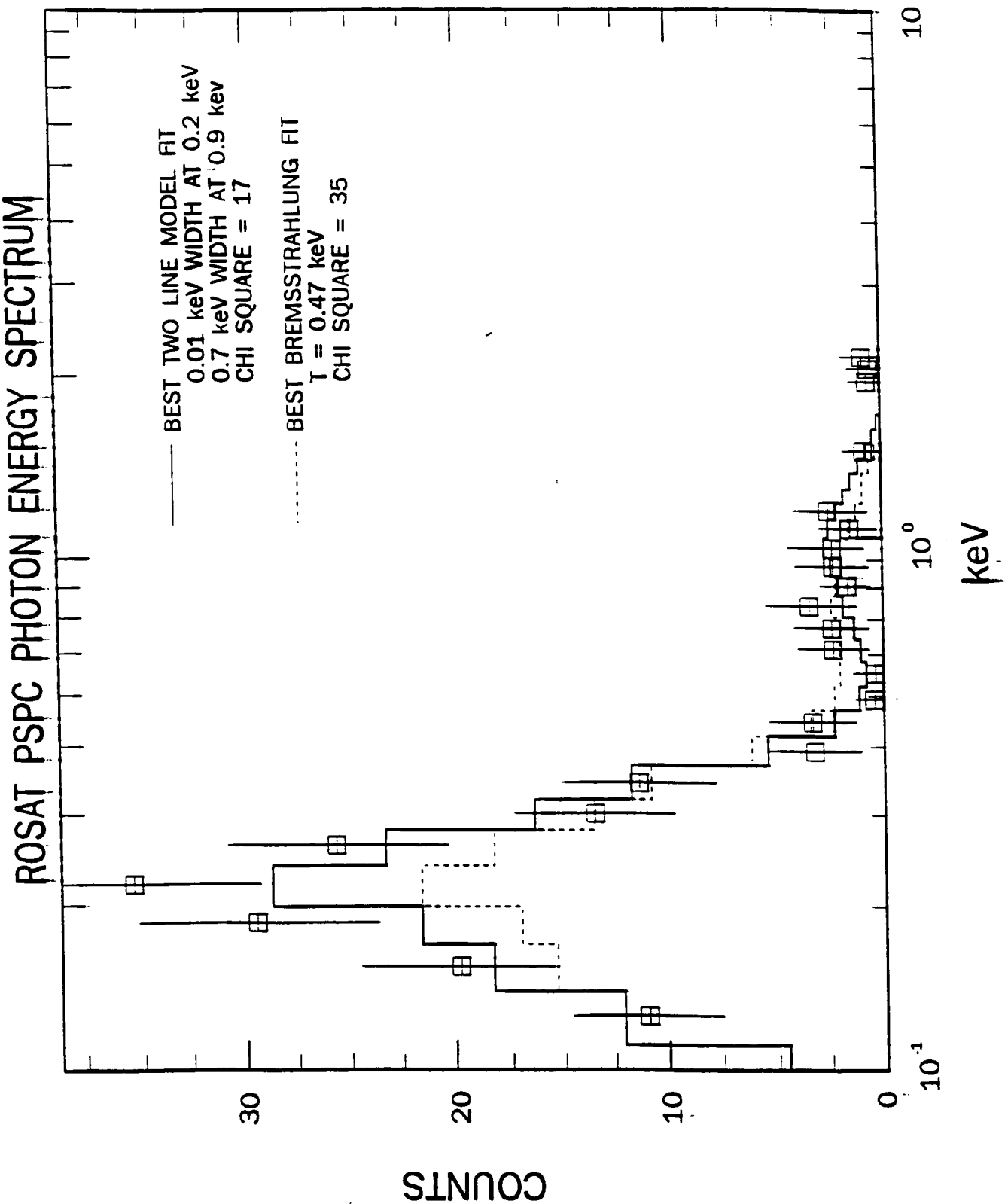
ROSAT PSPC PHOTON ENERGY SPECTRUM
BEST TWO LINE MODEL FIT
0.01 keV WIDTH AT 0.2 keV
0.7 keV WIDTH AT 0.9 kev
CHI SQUARE = 17
BEST BREMSSTRAHLUNG FIT
T = 0.47 keV
CHI SQUARE = 35
COUNTS
0
10
20
30
10^{-1}
10^{0}
10^{1}
keV

Figure 4

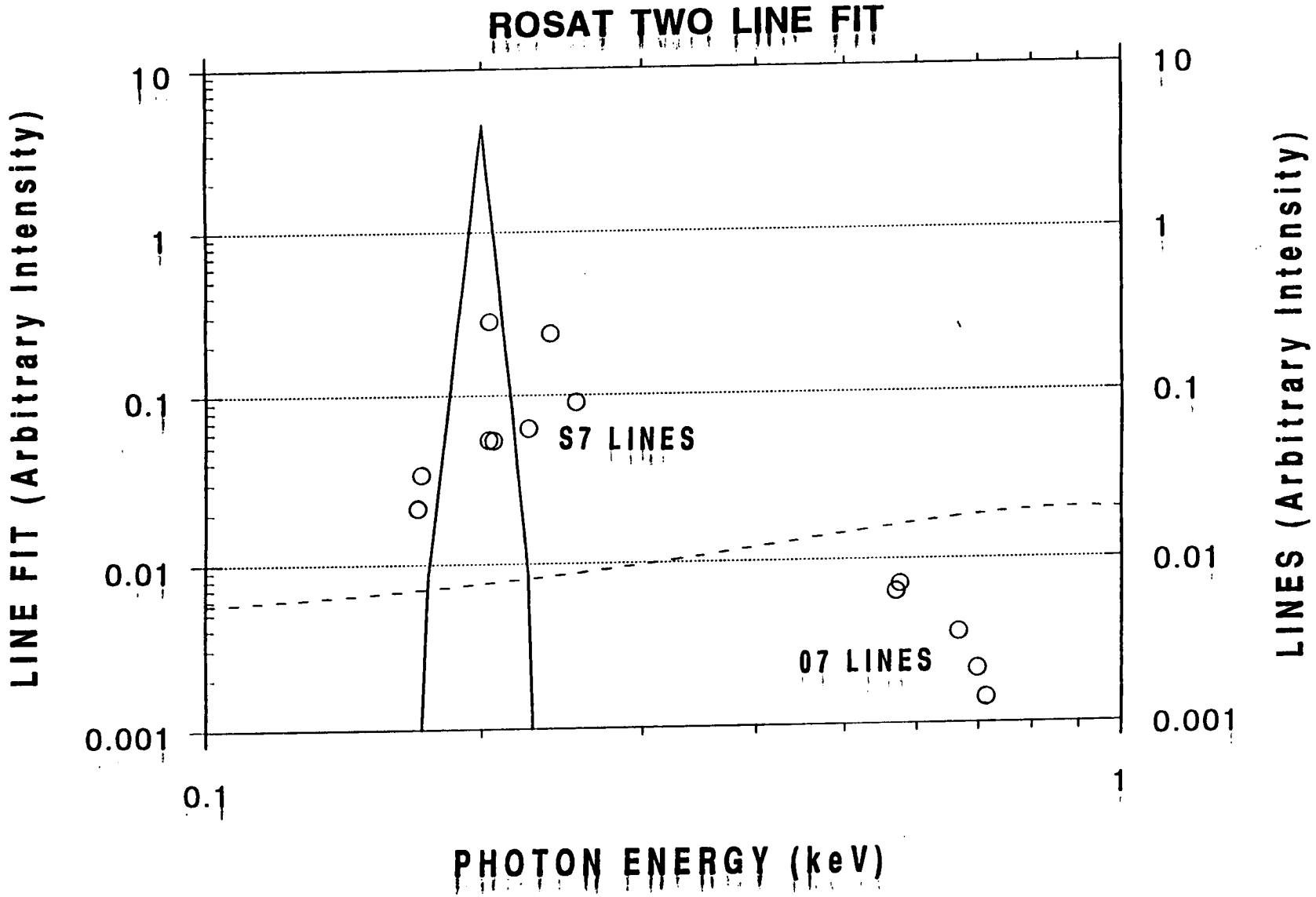
ROSAT TWO LINE FIT
LINE FIT (Arbitrary Intensity)
LINES (Arbitrary Intensity)
PHOTON ENERGY (keV)
10
1
0.1
0.01
0.001
0.1
1
S7 LINES
07 LINES

Figure 5

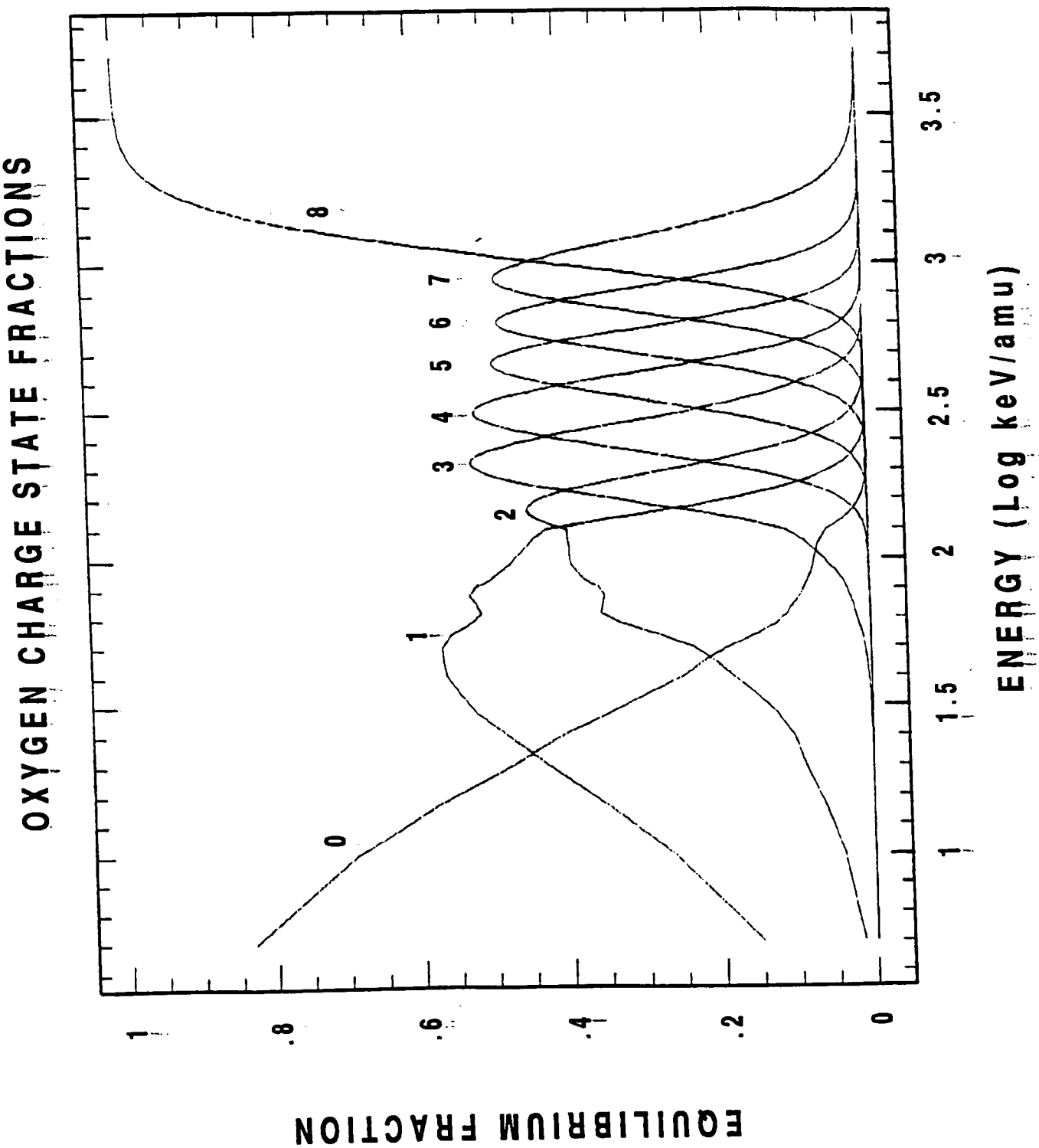
OXYGEN CHARGE STATE FRACTIONS
EQUILIBRIUM FRACTION
ENERGY (Log keV/amu)
0
1
2
3
4
5
6
7
8
1
1.5
2
2.5
3
3.5
.2
.4
.6
.8
1
0

Figure 6